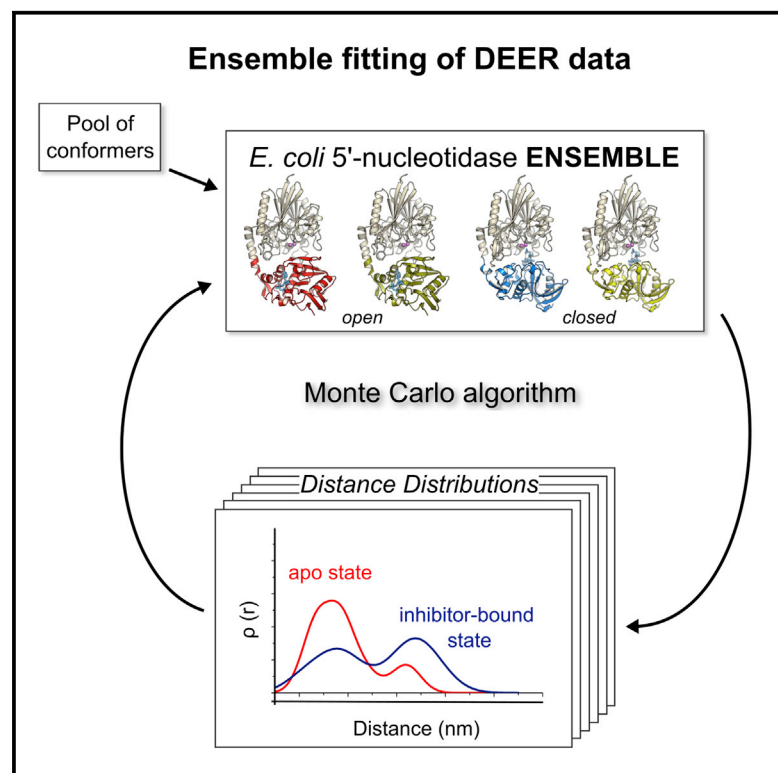


Structure

Characterization of the Domain Orientations of *E. coli* 5'-Nucleotidase by Fitting an Ensemble of Conformers to DEER Distance Distributions

Graphical Abstract



Authors

Ulrike Krug, Nathan S. Alexander, Richard A. Stein, Antje Keim, Hassane S. Mchaourab, Norbert Sträter, Jens Meiler

Correspondence

strater@bbz.uni-leipzig.de (N.S.), jens.meiler@vanderbilt.edu (J.M.)

In Brief

Krug et al. combine EPR distance distributions, information from crystal structures and an ensemble fitting procedure by a Monte Carlo search algorithm in an integrated study to describe the conformational population of *E. coli* 5'-nucleotidase in the apo- and inhibitor-bound states.

Highlights

- Almost isoenergetic states of a domain motion can be characterized by EPR
- X-Ray structures are combined with spectroscopic data by ensemble fitting
- A quantitative characterization of the equilibrium can be obtained
- Substrate binding changes the equilibrium from open to open and closed states



Characterization of the Domain Orientations of *E. coli* 5'-Nucleotidase by Fitting an Ensemble of Conformers to DEER Distance Distributions

Ulrike Krug,^{1,6} Nathan S. Alexander,^{2,3} Richard A. Stein,⁴ Antje Keim,¹ Hassane S. Mchaourab,^{2,4} Norbert Sträter,^{1,*} and Jens Meiler^{2,3,5,*}

¹Institute of Bioanalytical Chemistry, Center for Biotechnology and Biomedicine, University of Leipzig, Deutscher Platz 5, 04103 Leipzig, Germany

²Center for Structural Biology, Vanderbilt University, Nashville, TN 37212, USA

³Department of Chemistry, Vanderbilt University, Nashville, TN 37212, USA

⁴Department of Molecular Physiology and Biophysics, Vanderbilt University, Nashville, TN 37212, USA

⁵Vanderbilt University, 7330 Stevenson Center, Station B 351822, Nashville, TN 37235, USA

⁶Present address: Institute of Medical Physics and Biophysics, University of Leipzig, 04107 Leipzig, Germany

*Correspondence: strater@bbz.uni-leipzig.de (N.S.), jens.meiler@vanderbilt.edu (J.M.)

<http://dx.doi.org/10.1016/j.str.2015.11.007>

SUMMARY

Escherichia coli 5'-nucleotidase is a two-domain enzyme exhibiting a unique 96° domain motion that is required for catalysis. Here we present an integrated structural biology study that combines DEER distance distributions with structural information from X-ray crystallography and computational biology to describe the population of presumably almost isoenergetic open and closed states in solution. Ensembles of models that best represent the experimental distance distributions are determined by a Monte Carlo search algorithm. As a result, predominantly open conformations are observed in the unliganded state indicating that the majority of enzyme molecules await substrate binding for the catalytic cycle. The addition of a substrate analog yields ensembles with an almost equal mixture of open and closed states. Thus, in the presence of substrate, efficient catalysis is provided by the simultaneous appearance of open conformers (binding substrate or releasing product) and closed conformers (enabling the turnover of the substrate).

INTRODUCTION

Escherichia coli 5'-nucleotidase (5NT) belongs to the superfamily of calcineurin metallophosphatases (Knöfel and Sträter, 1999). It is a two-domain enzyme with a dimetal center located in the N-terminal domain where various substrates including nucleotides, nucleotide sugars, or dinucleotides are hydrolyzed (Glaser et al., 1967; Neu, 1967; Ruiz et al., 1989; Knöfel and Sträter, 1999, 2001b; Schultz-Heienbrok et al., 2005; Krug et al., 2013). Substrates bind to the C-terminal domain in the open state and a 96° rotation of this domain around its center enables hydrolysis via formation of the closed state (Figure 1). Substrate binding to

and product release from the open state are necessary for catalysis since the active site is occluded from solvent in the closed state (Schultz-Heienbrok et al., 2005). Due to the extensive domain rearrangement of the unique ball-and-socket-type motion and due to the availability of several crystal structures in different packing arrangements, 5NT is an excellent model enzyme for studying structure-function relationships of domain motions in catalysis.

By hydrolysis of extracellular nucleotides, bacterial 5NT provides nucleosides and phosphate as nutrients to the cell (Zimmermann, 1992). Furthermore, microbial pathogens impair immune functions of the infected hosts by generation of anti-inflammatory adenosine (Antonioli et al., 2013). 5NT activity was shown to interfere with host-immune responses for a number of bacterial microorganisms (Thammavongsa et al., 2009; Fan et al., 2012; Firon et al., 2014; Liu et al., 2014). Moreover, 5NT is the bacterial homolog of ecto-5'-nucleotidase (also known as CD73), an enzyme that is part of the purinergic signaling cascade where extracellular nucleotides or their degradation products interact with P2X, P2Y, and P1 receptors. CD73 activity is the dominant source of extracellular adenosine, a potent immunosuppressant. Notably, CD73 is overexpressed in several cancer cell lines (suppressing the immune response) and CD73 inhibitors are promising candidates for cancer immunotherapy (Zimmermann et al., 2012; Antonioli et al., 2013). Crystal structures show that CD73 undergoes a similar domain rearrangement as 5NT (Heuts et al., 2012; Knapp et al., 2012a, 2012b). 5NT has been captured in a total of 16 conformers by X-ray crystallography comprising open, closed, and intermediate states (Knöfel and Sträter, 1999, 2001a, 2001b; Schultz-Heienbrok et al., 2004, 2005). Here we set out to address the following questions via site-directed spin-labeling (SDSL) and electron paramagnetic resonance (EPR) spectroscopy: (1) Are the crystallographic conformers sufficient to characterize the conformational equilibrium in solution or do we observe additional conformers? (2) How is the equilibrium between open and closed states affected by ligand binding to the active site? (3) How many distance distributions are required to characterize the spatial arrangement of the two domains and the equilibrium of different

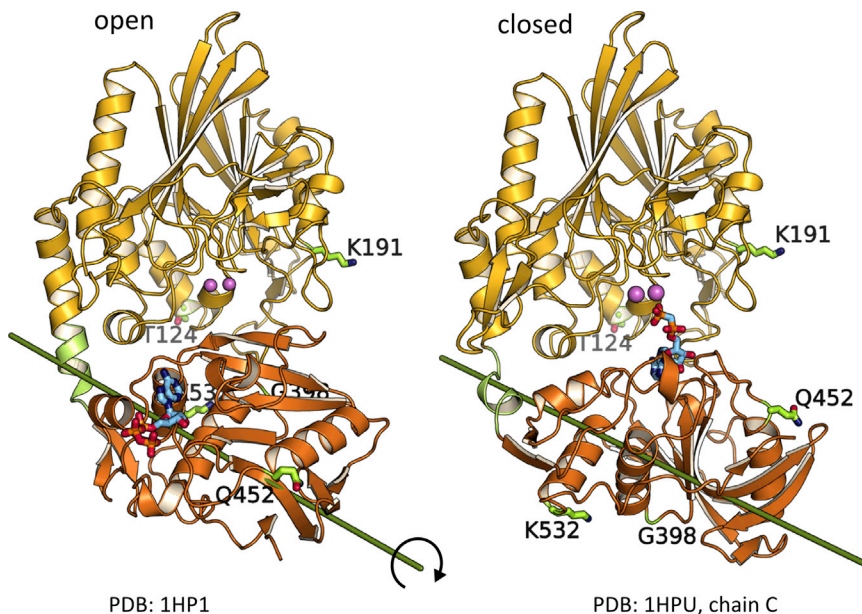


Figure 1. EPR Spin Label Positions in the Open and Closed Crystal Structures of 5NT

The N-terminal domain (yellow) contains the di-metal center (pink), the C-terminal domain (orange) contains the substrate binding pocket. The rotation axis between the open and closed states is indicated. For EPR studies, six double cysteine variants (with one cysteine in each domain) were prepared (see also Figure S1). The labeling sites are indicated by the original amino acid side chain (before the mutation) depicted as sticks.

tive orientation and translation of 5NT's two domains, i.e., two rigid bodies. In this study, five labeling sites (T124C, K191C, G398C, Q452C, K532C) were selected constituting a set of six residue pairs with a preference for observing large changes in distances in orthogonal directions. Thus, the number of residue pairs is at a minimum to define the relative orientation of two completely independent

states? (4) To what extent do the spin labels influence the equilibrium, which might involve almost isoenergetic states?

An integrated structural biology approach was used to answer these questions and define the conformational dynamics. Spin label sites to measure distances by double electron-electron resonance spectroscopy (DEER) were specifically selected to capture the domain motion postulated by the crystal structures. To quantitatively analyze the DEER distance distributions, which report dynamic modes that modulate the distance between two labels (Mchaourab et al., 2011; Jeschke, 2012), we developed a Monte Carlo search algorithm that reproduces experimental distributions in terms of the underlying populations in a self-consistent manner by selecting conformers from a pool of structures. Different initial pools with increasing structural diversity (i.e., crystal structure conformers, models from molecular dynamics [MD] or from docking of the domains) were used to find the best fit to the distance distributions. Furthermore, implicit and explicit spin label representations were compared. Finally, by the introduction of a leave-one-out procedure, we developed a strategy to avoid overfitting the structure ensembles to the experimental data and to demonstrate the predictive power of the ensembles.

RESULTS

EPR Reveals Conformational Changes upon Addition of Inhibitor

SDSL methods in combination with EPR distance measurements are widely used to characterize the structure-function relationships of proteins (Hubbell et al., 2000; Columbus and Hubbell, 2002; Fanucci and Cafiso, 2006). Covering a distance range between 20 and 80 Å, they constitute an ideal way to obtain information about the inter-domain orientation in modular proteins (Ward et al., 2009) or can be used to dock protein complexes on the basis of distance distributions (Edwards et al., 2014). Six free parameters are required to characterize the rela-

rigid bodies. However, the use of docked models, models along a simulated path between open and closed states, and the crystallographically observed states significantly reduces the degrees of freedom of the system to be characterized. The resulting six double cysteine mutants T124C/G398C, T124C/Q452C, T124C/K532C, K191C/G398C, K191C/Q452C, and K191C/K532C (Figures 1 and S1) showed a specific activity of 70%–120% of that of wild-type 5NT. Labeling with methanethiosulfonate spin labels (MTSSLs) did not significantly alter these values. Thus, the modification and the labeling did not disturb catalysis.

Crystal structures of 5NT in complex with the non-hydrolyzable ADP analog adenosine 5'-(α,β -methylene)diphosphate (AMPCP) show that the inhibitor binds between the two enzyme domains in a conformation that probably corresponds to the catalytically competent Michaelis complex (Knöfel and Sträter, 2001b). Thus, protein samples of inhibitor-free (apo) and inhibitor-bound states, i.e., after addition of saturating amounts of AMPCP and Zn^{2+} (ZnAMPCP), were investigated. Dipole-dipole couplings between the introduced MTSSLs were measured with DEER, and the distance distributions (Figures 2 and S2) were derived utilizing Tikhonov regularization (Chiang et al., 2005). All mutants showed a shift of the distance distribution between the apo and the ZnAMPCP state indicating a conformational change upon addition of inhibitor. Depending on the positions of the spin labels, the distances increased or decreased with the domain closure motion. Although the distance distributions differ in the number of observed maxima, the height of the peaks, and their broadness, all apo states sampled predominantly monomodal distributions with maxima indicative of the open conformations. In contrast, in the ZnAMPCP states, multimodal distance distributions were observed corresponding to a mixture of different states. Also, there was very little change in the continuous wave (CW) EPR spectra (Figure S2) under the different conditions, supporting large-scale protein reorientation for the changes seen in the DEER experiments and minimal change in the local environment of the spin label upon domain closure.

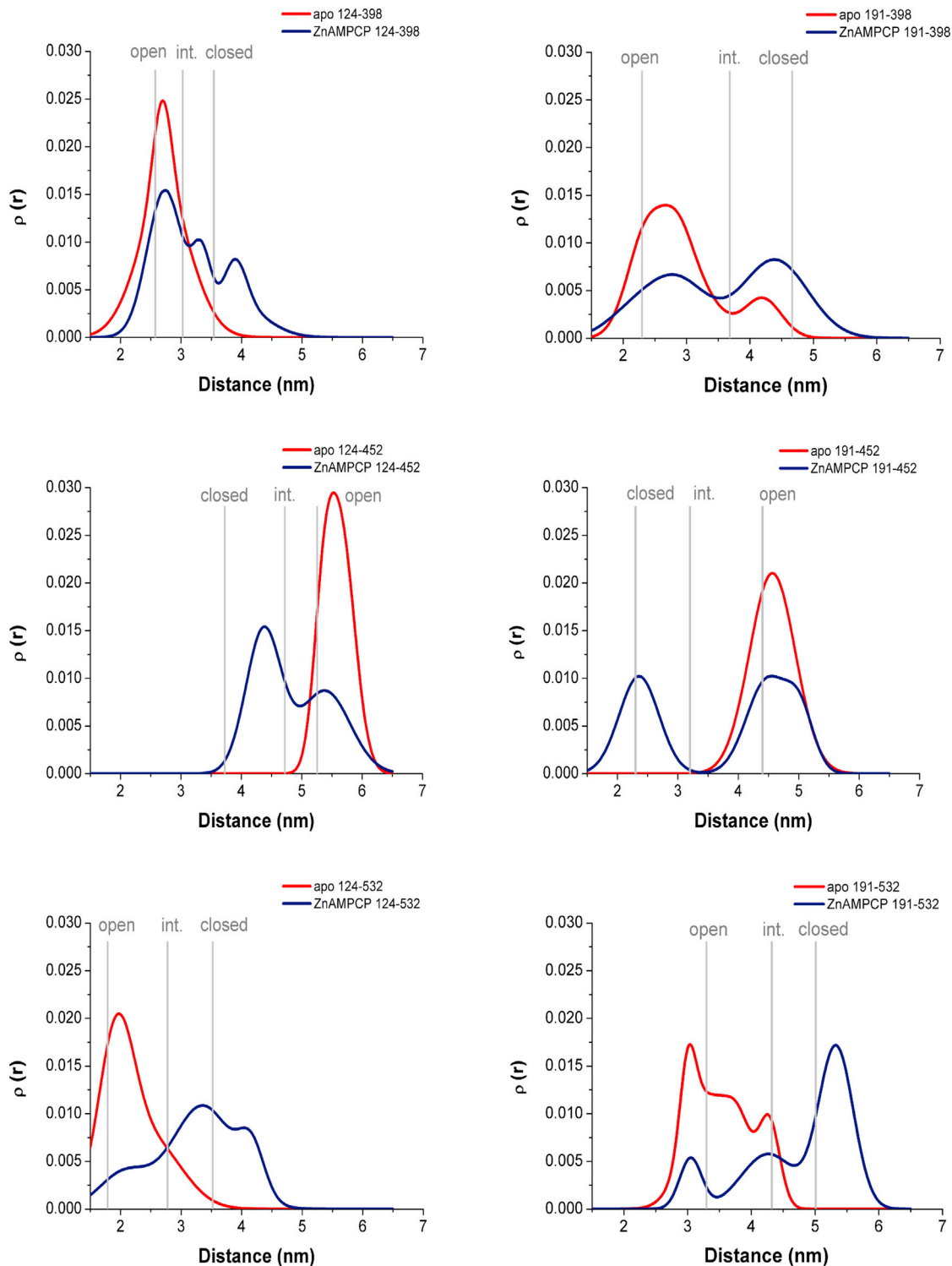


Figure 2. DEER Distance Distributions of Six MTSSL Labeled 5NT Mutants

The apo (red) and the ZnAMPCP bound state (blue) are compared. Labeling positions are indicated. Gray bars mark the expected distances of the spin labels in the crystallographically open, intermediate, and closed states (as estimated from theoretical distance distributions of all crystal structure conformers calculated with the rotamer library using the program MMM; see also [Figure S3](#)) ([Polyhach et al., 2011](#)). For CW-EPR data and DEER traces, compare [Figure S2](#).

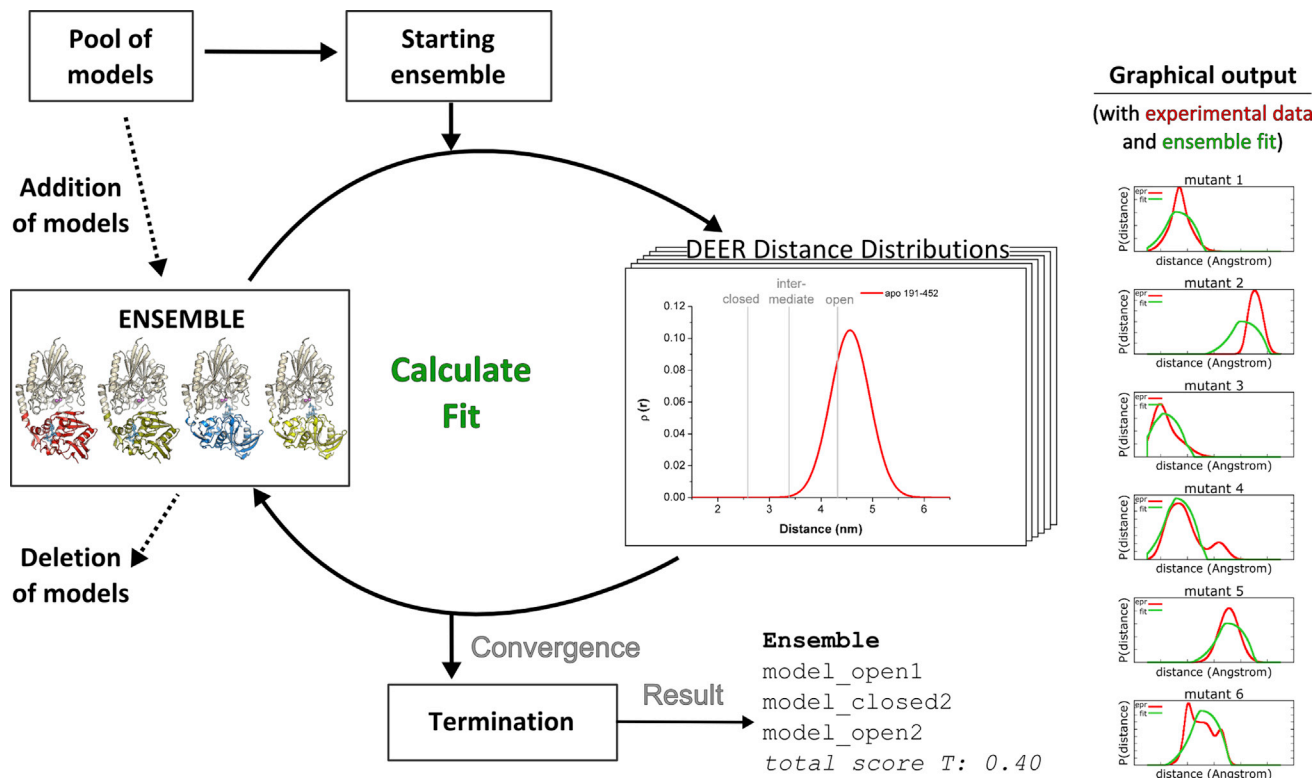


Figure 3. Scheme for Ensemble Fitting of 5NT Distance Distributions

An initial starting ensemble is randomly selected from a pool of models by a Monte Carlo search algorithm to describe the experimental data. Then, during optimization, models are added to and/or deleted from the ensemble until the termination criterion is fulfilled. As output, an ensemble, a score, and a graphical comparison of the experimental data and the fit by the ensemble are given. See [Experimental Procedures](#) and [Figure S4](#).

A comparison of the broadness and shape of the experimental distance distributions in the open enzyme with distributions simulated based on the rotamer library, as implemented in MMM (Polyhach et al., 2011), showed that the experimental distributions mostly have less maxima or a less pronounced fine structure of narrow peaks (Figure S3). After averaging the simulated distance distributions of the seven open crystal forms, the shape of the resulting averaged distance distribution was more similar to the experimental observations. Previous work (Polyhach et al., 2011; Alexander et al., 2013) has shown that distance distributions obtained with the MMM rotamer library overestimate the breadth of tight distributions. Therefore, the good match of the averaged distributions and the experimental data would suggest that the $\sim 10^\circ$ of inter-domain flexibility within the open or closed states of 5NT (Knöfel and Sträter, 2001a) contributes to the overall width of the distributions.

Ensemble Fitting to Characterize Conformational Ensembles

An ensemble fitting procedure was employed for a quantitative description of the conformational population in the apo and the ZnAMPCP states, (Figure 3). A starting ensemble was randomly chosen from the pool of models. To improve the fit of the distance distributions, further models were added, replaced, or removed from the ensemble based on a Monte Carlo algorithm. The total score T served as a quality indicator for the fits. To ac-

count for the flexibility of the spin label, the probability function of the knowledge-based potential from the motion-on-a-cone model (Alexander et al., 2008; Hirst et al., 2011) and in a second approach, full-atom representations derived from RosettaEPR (Alexander et al., 2013) were used. This allowed for a comparison of implicit versus explicit spin label representations.

Generation and Description of the Models in the Pool for Fitting to the Distance Distributions

Crystal Structure Conformers

Sixteen available crystallographic conformers were used for ensemble fitting. For a comprehensive description of the relationship between these conformers, they are described relative to models from an artificial linear path (i.e., rotation around a single axis) between the most open and the most closed conformers. This is helpful as two conformers can have a similar rotation angle relative to the most closed conformer 1HPU_C, but are not necessarily the same. The aim of this linear path analysis is to describe differences between two conformers in more detail than by the calculation of rotation angles relative to only one reference conformer (Knöfel and Sträter, 2001a; Schultz-Heienbrok et al., 2004). For a given conformer, the angle χ_1 describes the inter-domain rotation angle of the most similar conformer on the linear rotation path between the open and closed states. χ_2 represents the tilt angle of the analyzed conformer to the most similar conformer on the linear

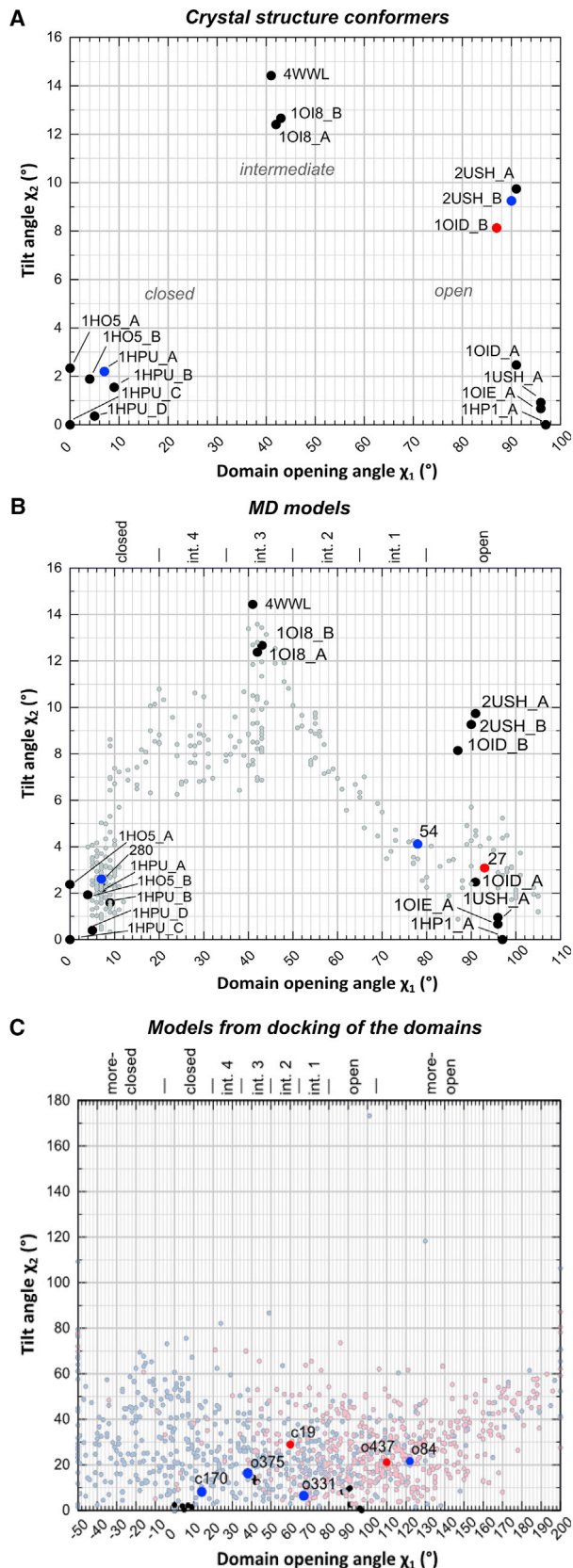


Figure 4. χ_1, χ_2 Plots of 5NT Crystal Structures, MD Models, and Models from Docking of the Two Domains

(A–C) χ_1 describes the domain opening angle on the 1HPU_C-1HP1-rotation. χ_2 is the tilt angle relative to the reference state. Crystal structure conformers are shown as filled circles (black) in all panels. Conformers that were found by ensemble fitting to describe the experimental DEER distance distribution with the cone model at $w_E = 40$ are indicated as red (apo) and blue points (ZnAMPCP) and by their model ID. In (C), models from docking of the two domains were prepared with 1HPU_C (closed, light blue) and with 1HP1_A (open, light red). For definitions of the conformers in (B) and (C), see also Tables S1 and S2.

path, i.e., the deviation of the conformer from the linear path (see [Experimental Procedures](#) for further details).

The two-dimensional plot of the angles χ_1 and χ_2 shows that the crystallographically observed open and closed conformers each span a χ_1 range of about 10° on the linear path (Figure 4A). Furthermore, the open crystallographic conformers show a tilt angle χ_2 up to 10° , whereas the closed conformations are more similar to each other with $\chi_2 \leq 3^\circ$. The intermediate conformations with $\chi_1 \approx 45^\circ$ show the highest tilt from the linear path with $\chi_2 \approx 14^\circ$, which is a result from steric clashes (U.K., N.S., unpublished data).

The description of the conformational space of the crystal conformers is limited to a set of seven open, three intermediate, and six closed conformations. Further conformers were generated in silico, either by targeted MD simulation or by docking of the two domains, to test if additional conformations improve the fit of the experimental data.

MD Models

Figure 4B shows the χ_1, χ_2 plot of the models generated by a targeted MD simulation between the open and closed state to fill in the gaps between the crystal structures. The simulated domain rearrangement between the open and closed conformers takes a path via the crystallographically observed intermediate conformations (U.K., N.S., unpublished data).

Docked Models

To generate an even larger conformational diversity in the model pool, we built models with different domain orientations via a docking algorithm. About 22% of the models have a domain orientation similar to that of the crystal structures, i.e., with $-5^\circ \leq \chi_1 \leq 105^\circ$ and $\chi_2 \leq 20^\circ$. The other models are, according to their χ_1 values, more closed or more open and/or their tilt angle from the linear path is considerably higher ($\chi_2 > 20^\circ$) than that of the crystal structures (Figure 4C). We found it necessary to prepare models starting from an open (1HP1_A) as well as a closed (1HPU_C) conformation as the resulting docked models cluster in distinct regions of the plot. This is likely caused by local structural differences predominantly located in the N-terminal domain of 5NT. In 1HP1_A residues 323–331 are not defined, in 1HPU_C they form a β -hairpin structure. Furthermore, residues of the 180s loop that is located at the domain interface undergo a conformational change between the two states (Knöfel and Sträter, 1999).

Validation of Ensemble Fitting and Determination of the Optimal Ensemble Size Score

To evaluate the results of ensemble fitting with respect to the possibility of overfitting, a free score S_{free} was introduced as a quality indicator (Figure 5A). S_{free} was determined by the

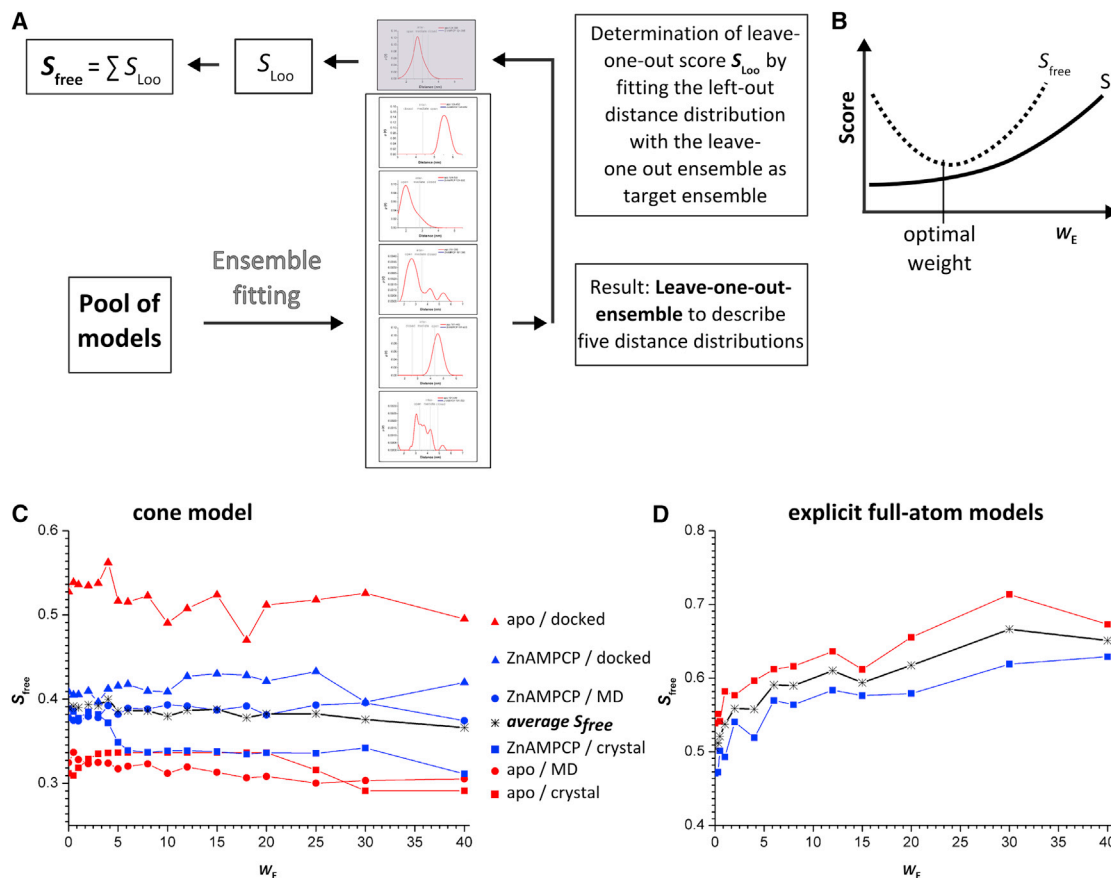


Figure 5. Determination of the Optimal Ensemble Size by Variation of the Penalty Factor w_E

S_{free} describes the goodness of the fit to the distance distributions using a leave-one-out procedure.

(A) Scheme for determination of S_{free} .

(B) Expected dependency of the calculated S and S_{free} on the weight of the ensemble size (w_E). The minimum of S_{free} defines the optimal w_E .

(C and D) Dependency of S_{free} on w_E for ensemble fitting with the cone model or explicit full-atom models. Each curve represents the average of the best 10% of the fits. The minimum of all curves, i.e., of the average S_{free} , is obtained at $w_E = 40$ for the cone model and $w_E = 0$ for the full-atom models (see also Figure S5).

leave-one-out approach and is the sum of six leave-one-out scores (S_{Loo}). First, with S_{free} the optimal ensemble size N was evaluated. The total score T is defined by $T = S + w_E E$, where S is the comparison to the EPR distance distributions and E represents the ensemble size score, which is given as N , the number of models in the ensemble, divided by P , the total number of models in the pool. The weighting term (w_E) serves as a penalty score for N in the fitting procedure. A large number of models (i.e., allowed by a low w_E) may improve the fit to the observed distance distributions (decrease of S) but will at some point result in overfitting (increasing S_{free} ; Figure 5B). Indeed, for all fits with the cone model as well as with the full-atom spin label, the number of models in the ensemble decreased strongly with increasing w_E (see Figure S5). However, the dependency of S and S_{free} on the ensemble size was found to be different for implicit (cone model) and explicit (full-atom) spin labels. For the cone model, the average of the fittings for the two datasets (apo and ZnAMPCP) with the three different pools of models showed only a small dependency of S and S_{free} on the ensemble size (Figures 5C and S5). The best results were obtained with $w_E = 40$, the highest weighting term tested here. Further calcula-

tions with $w_E > 40$ were not employed because the ensemble size was generally already at a minimum for the crystal structures and the MD models ($N = 1$ for the apo structure and $N = 2$ for the AMPCP-liganded enzyme) at this penalty weight (see below). In the following, the ensembles were analyzed for the conditions that resulted in the lowest S_{free} values, i.e., at $w_E = 40$.

Analysis of the Ensemble Fitting with the Cone Model

To describe the conformational population of 5NT in solution, the six experimental distance distributions were fitted based on the knowledge-based potential of the cone model (Table 1, Figure 4). Comparing the results shows that the fitting scores decreased (i.e., improve) with the inclusion of more diverse models, i.e., $S(\text{crystal structures}) > S(\text{MD models}) > S(\text{docked models})$, while S_{free} was increasing in this order (Table 1). $S_{\text{free}}(\text{crystal structures})$ and $S_{\text{free}}(\text{MD models})$ were similar only for the apo data with $S_{\text{free}} \approx 0.3$. Thus, the inclusion of additional conformers as generated by the directed MD simulation did not improve the fits of the apo data significantly or resulted in overfitting as in the case of the ZnAMPCP data and the docked models. From this, we conclude that the crystal conformers are sufficient

to describe the distance distributions based on the available data size of six distance distributions and the accuracy of the data.

We also evaluated how well each of the 16 crystal structure conformers alone fits the experimental distance distributions (Table 2). This analysis clearly reveals that, compared with the open conformations (with $S \approx 0.3$), intermediate (with $S > 1.0$) and closed conformations (with $S \approx 2$) are not appropriate to solely describe the apo data. 1OID_B exhibits the best fit ($S = 0.29$). This conformer was also selected in the ensemble fittings with $w_E = 40$ (Figure S4). The ensembles based on the MD model pool likewise consist of only one open conformer for the apo data. Thus, on the basis of the refinements against the crystal and MD conformers, we conclude that the apo state comprises almost exclusively open conformations. Although intermediate conformers were observed for the docked models (~43%), no conformation with a rotation angle χ_1 less than 50° is included in the final ensemble (Table 1). This indicates that the enzyme does not adopt the closed state to a measurable extent in the absence of substrate/inhibitor. Furthermore, as the SD in the fits of the docked models are generally high and S_{free} indicates overfitting, we do not consider the finding of non-open conformers as a definite indication of the existence of such states. The same is concluded for the finding of more open conformers ($\chi_1 > 105^\circ$) in the final ensembles for the apo and the ZnAMPCP data.

Furthermore, in the fits with the crystal structures, the open model 1OID_B was found for the apo data and the open model 2USH_B for the ZnAMPCP data. However, we assume that this is no indication for different open states in the presence or absence of nucleotide as the models are exchangeable with no significantly worse S (not shown). Fitting of the apo data with the docked models at $w_E = 40$ yielded ensembles with at least two models (Figure S4). By increasing to $w_E = 400$, the ensemble size was reduced to one model to determine how similar the resulting docked models would be to the crystallographic open conformers if only a single conformer is available to fit the distance distributions. Out of ten different solutions, the best fit is represented by a more open conformation ($\chi_1 = 110^\circ$, $\chi_2 = 21.2^\circ$). But also an open conformer ($\chi_1 = 94^\circ$, $\chi_2 = 2.9^\circ$) is among the best 10% of the fits, which is very similar to the crystallographic open states. This finding corroborates the notion that the crystallographically observed open conformers are also present in solution. It also shows that this state can be modeled with very good accuracy based only on the docked models. We assume that the other more diverse solutions may be avoided by including more distance distributions or by a less flexible spin label. For the ZnAMPCP state, no single crystal conformer is sufficient to obtain a good fit to the experimental distance distributions (Table 2). The best score of $S = 0.51$ obtained for the intermediate conformer 1OI8_A is significantly worse than $S = 0.31$ for an ensemble of one open (2USH_B) and one closed structure (1HPU_A) after fitting with all available crystal structure conformers (Figures 4 and S4). Thus, the inclusion of at least two conformers in the ensemble is required for a reasonable characterization of the inhibitor-bound state. Indeed, all ensembles describing the ZnAMPCP-bound state are a mixture of different conformers. Based on the crystal conformers, a 1:1 equilibrium of open and closed conformations is observed with low SD. As

the variability of the models increases with MD and docked models, the resulting ensembles become more diverse and contain more intermediates (Table 1). However, the SD for the ratio of the different conformations in these ensembles is mostly relatively high and the inclusion of the more diverse models does not improve the quality of the fits but results in a significantly increased S_{free} for the docked models. For the refinement against the docked models, the number, accuracy, and independence of the six distance distributions (including influences of the spin labels on the equilibrium of states) does not allow for an unrestrained determination of an equilibrium of different domain orientations. Thus, a decrease of restraints and an increase of conformational diversity (crystal conformers \rightarrow MD conformers \rightarrow docked conformers) results in a more diverse final ensemble and thus larger SDs.

Fitting of the Distance Distributions with Explicit Full-Atom Spin Labels

In a second approach, ensemble fitting was performed with full-atom models of MTSSL attached to the crystal structure conformers instead of using the probability function of the cone model to describe the conformational space of the label. First, the optimal w_E was determined, as was done for the cone model. Ensemble fitting with the explicit spin labels showed a higher dependency on w_E and the minimum was found at $w_E = 0$ (Figures S5 and S5). In addition, there are three major differences compared with the fits with the cone model (Table 3): (1) the optimal weighting term was $w_E = 0$, leading to an increased number of conformers in the final ensemble, (2) S was lower while S_{free} was higher, and (3) more intermediate conformers were used to describe the ZnAMPCP state. Although exclusion of the intermediates from the initial pool results in a worse fit ($S_{\text{free}} = 0.59 \pm 0.05$ compared with $S_{\text{free}} = 0.47 \pm 0.03$ with intermediate conformers), S_{free} is still significantly increased compared with the fits with the cone model. Thus, we do not consider this as proof for the existence of the intermediate conformations in the ZnAMPCP state.

Overall the cone model appears better suited for regularizing the fitting protocol to prevent overfitting.

Evaluation of the Labeling Sites

S_{LOO} allows for an evaluation of the contribution of each distance distribution to the overall fit (Tables 1 and 3). It may reveal if a variant was not perfectly chosen by displaying a higher S_{LOO} compared with the other variants. Only the mutant 124/452 showed increased S_{LOO} values for some fits (compare Table 1). A reason may be the higher mobility of the spin label probe as residue 452 is located in a flexible region and not in a secondary structure element. This is also reflected in increased residual B factors relative to the domains (data not shown). On the other hand, 124/452 is not an outlier in all fits (compare also Table 3) and the ensembles selected in the LOO calculations are mostly very similar (Table S3). This indicates the significance of the fits and the absence of overfitting. In addition, as described above, the CW-EPR data (Figure S2) do not point to increased spin label flexibility and any serious problems with any of the mutants. Thus, all mutants contribute with their EPR distance distributions to the differentiation between apo and bound states.

Table 1. Description of the Conformational States of 5NT by Ensemble Fitting with Different Pools of Models Using the Cone Model

Scores \pm SD	Apo	Open	Intermediate	Closed					
<i>Fit with crystal structures</i>									
$S = 0.2911 \pm 0.0000$	all six	100%	0%	0%					
$S_{\text{LOO}} = 0.0338 \pm 0.0000$	LOO 124/398	100%	0%	0%					
$S_{\text{LOO}} = 0.1062 \pm 0.0000$	LOO 124/452	100%	0%	0%					
$S_{\text{LOO}} = 0.0315 \pm 0.0000$	LOO 124/532	100%	0%	0%					
$S_{\text{LOO}} = 0.0453 \pm 0.0000$	LOO 191/398	100%	0%	0%					
$S_{\text{LOO}} = 0.0265 \pm 0.0000$	LOO 191/452	100%	0%	0%					
$S_{\text{LOO}} = 0.0477 \pm 0.0000$	LOO 191/532	100%	0%	0%					
$S_{\text{free}} = 0.2910 \pm 0.0000$	average ratio	100%	0%	0%					
ZnAMPCP									
$S = 0.3110 \pm 0.0000$	all six	50%	0%	50%					
$S_{\text{LOO}} = 0.0195 \pm 0.0000$	LOO 124/398	50%	0%	50%					
$S_{\text{LOO}} = 0.0772 \pm 0.0000$	LOO 124/452	50%	0%	50%					
$S_{\text{LOO}} = 0.0594 \pm 0.0000$	LOO 124/532	50%	0%	50%					
$S_{\text{LOO}} = 0.0192 \pm 0.0000$	LOO 191/398	50%	0%	50%					
$S_{\text{LOO}} = 0.0476 \pm 0.0000$	LOO 191/452	50%	0%	50%					
$S_{\text{LOO}} = 0.0884 \pm 0.0006$	LOO 191/532	50%	0%	50%					
$S_{\text{free}} = 0.3110 \pm 0.0006$	average ratio	50%	0%	50%					
Scores \pm SD	Apo	Open	Intermediate 1	Intermediate 2	Intermediate 3	Intermediate 4	Closed		
		$106^\circ \leq \chi_1 \leq 80^\circ$	$80^\circ < \chi_1 \leq 65^\circ$	$65^\circ < \chi_1 \leq 50^\circ$	$50^\circ < \chi_1 \leq 35^\circ$	$35^\circ < \chi_1 \leq 20^\circ$	$20^\circ < \chi_1 \leq 0^\circ$		
<i>Fit with MD models</i>									
$S = 0.2689 \pm 0.0000$	all six	100%	0%	0%	0%	0%	0%		
$S_{\text{LOO}} = 0.0250 \pm 0.0000$	LOO 124/398	100%	0%	0%	0%	0%	0%		
$S_{\text{LOO}} = 0.1070 \pm 0.0020$	LOO 124/452	100%	0%	0%	0%	0%	0%		
$S_{\text{LOO}} = 0.0268 \pm 0.0000$	LOO 124/532	100%	0%	0%	0%	0%	0%		
$S_{\text{LOO}} = 0.0678 \pm 0.0000$	LOO 191/398	100%	0%	0%	0%	0%	0%		
$S_{\text{LOO}} = 0.0229 \pm 0.0000$	LOO 191/452	100%	0%	0%	0%	0%	0%		
$S_{\text{LOO}} = 0.0557 \pm 0.0000$	LOO 191/532	100%	0%	0%	0%	0%	0%		
$S_{\text{free}} = 0.3052 \pm 0.0020$	average ratio	100% \pm 0	0%	0%	0%	0%	0%		
ZnAMPCP									
$S = 0.2690 \pm 0.0027$	all six	0%	50%	0%	0%	0%	50%		
$S_{\text{LOO}} = 0.0402 \pm 0.0036$	LOO 124/398	0%	50%	0%	0%	0%	50%		
$S_{\text{LOO}} = 0.0583 \pm 0.0082$	LOO 124/452	0%	50%	0%	0%	0%	50%		
$S_{\text{LOO}} = 0.0559 \pm 0.0010$	LOO 124/532	50%	0%	0%	0%	0%	50%		
$S_{\text{LOO}} = 0.0445 \pm 0.0024$	LOO 191/398	0%	50%	0%	0%	0%	50%		
$S_{\text{LOO}} = 0.0865 \pm 0.0008$	LOO 191/452	0%	50%	0%	0%	0%	50%		
$S_{\text{LOO}} = 0.0888 \pm 0.0048$	LOO 191/532	50%	0%	0%	0%	0%	50%		
$S_{\text{free}} = 0.3742 \pm 0.0208$	average ratio	14% \pm 24%	36% \pm 24%	0%	0%	0%	50% \pm 0		
Scores \pm SD	Apo	More Open	Open	Intermediate 1	Intermediate 2	Intermediate 3	Intermediate 4	Closed	More closed
		$\chi_1 > 105^\circ$	$105^\circ \leq \chi_1 \leq 80^\circ$	$80^\circ < \chi_1 \leq 65^\circ$	$65^\circ < \chi_1 \leq 50^\circ$	$50^\circ < \chi_1 \leq 35^\circ$	$35^\circ < \chi_1 \leq 20^\circ$	$20^\circ < \chi_1 \leq -5^\circ$	$-5^\circ > \chi_1$
<i>Fit with docked models</i>									
$S = 0.2394 \pm 0.0074$	all six	50%	0%	0%	50%	0%	0%	0%	0%
$S_{\text{LOO}} = 0.0684 \pm 0.0193$	LOO 124/398	50%	0%	0%	50%	0%	0%	0%	0%
$S_{\text{LOO}} = 0.1017 \pm 0.0345$	LOO 124/452	50%	0%	0%	50%	0%	0%	0%	0%

(Continued on next page)

Table 1. Continued

Scores \pm SD	Apo	More Open	Open	Intermediate 1	Intermediate 2	Intermediate 3	Intermediate 4	Closed	More closed
		$\chi_1 > 105^\circ$	$105^\circ \leq \chi_1 \leq 80^\circ$	$80^\circ < \chi_1 \leq 65^\circ$	$65^\circ < \chi_1 \leq 50^\circ$	$50^\circ < \chi_1 \leq 35^\circ$	$35^\circ < \chi_1 \leq 20^\circ$	$20^\circ < \chi_1 \leq -5^\circ$	$-5^\circ > \chi_1$
$S_{\text{LOO}} = 0.0852 \pm 0.0161$	LOO 124/ 532	50%	0%	0%	50%	0%	0%	0%	0%
$S_{\text{LOO}} = 0.0995 \pm 0.0000$	LOO 191/ 398	100%	0%	0%	0%	0%	0%	0%	0%
$S_{\text{LOO}} = 0.1069 \pm 0.0415$	LOO 191/ 452	50%	0%	0%	50%	0%	0%	0%	0%
$S_{\text{LOO}} = 0.0335 \pm 0.0092$	LOO 191/ 532	50%	0%	0%	50%	0%	0%	0%	0%
$S_{\text{free}} = 0.4952 \pm 0.1206$	average ratio	$57\% \pm 19\%$	0%	0%	$43\% \pm 19\%$	0%	0%	0%	0%
ZnAMPCP									
$S = 0.2222 \pm 0.0120$	all six	25%	0%	25%	0%	25%	0%	25%	0%
$S_{\text{LOO}} = 0.0348 \pm 0.0113$	LOO 124/ 398	25%	0%	25%	0%	0%	25%	25%	0%
$S_{\text{LOO}} = 0.0841 \pm 0.0170$	LOO 124/ 452	25%	25%	0%	0%	0%	25%	25%	0%
$S_{\text{LOO}} = 0.0194 \pm 0.0103$	LOO 124/ 532	25%	25%	0%	0%	0%	25%	25%	0%
$S_{\text{LOO}} = 0.0776 \pm 0.0180$	LOO 191/ 398	0%	0%	25%	25%	25%	0%	25%	0%
$S_{\text{LOO}} = 0.1159 \pm 0.0165$	LOO 191/ 452	25%	0%	25%	0%	25%	25%	0%	0%
$S_{\text{LOO}} = 0.0880 \pm 0.0244$	LOO 191/ 532	0%	33%	0%	0%	33%	0%	0%	33%
$S_{\text{free}} = 0.4198 \pm 0.0975$	average ratio	$18\% \pm 12\%$	$12\% \pm 15\%$	$14\% \pm 13\%$	$4\% \pm 9\%$	$15\% \pm 15\%$	$14\% \pm 13\%$	$18\% \pm 12\%$	$5\% \pm 13\%$

S and S_{LOO} are given as average of the best 10% of the fits with their SD at $w_E = 40$. S_{free} is the sum of the six S_{LOO} . The conformational population of the best fit is given for each pool of models (see also Table S3).

DISCUSSION

The Conformational Switch in 5NT Catalysis

In the present study, we demonstrate the use of distance distributions from SDSL-EPR spectroscopy to study the conformational population of the domain orientations of 5NT in solution via an ensemble fitting approach. In the apo state, 5NT is present in open conformations. Then, the enzyme's active site is accessible for substrate binding; the molecules are in a ready-to-go conformation. In the presence of the inhibitor AMPCP, a mixture of different conformations is observed. About half of the enzyme is in the closed state and half in the open state. The non-hydrolyzable ADP substrate analog binds with its base to the C-terminal domain and with the phosphonate groups to the metal ion and the side chains of the N-terminal domain. Thus, the conformational change is caused by these interactions stabilizing predominantly the closed state, presumably via conformational selection. However, the present data cannot exclude that AMPCP binding contributes kinetic-induced fit effects to enable the closure motion. The fact that the closed state of the enzyme could be observed in previous crystal structures in the absence of bound inhibitors (Knöfel and Sträter, 2001b) indicates that a

small percentage of the unliganded enzyme also exists in the closed state. This percentage is below the detection limit achieved in this work. Furthermore, we could not find any definite indication of the existence of intermediate conformers in the apo or the ZnAMPCP-bound states as the sampling of intermediate structures was always accompanied by high SD which indicated overfitting.

Comparison of Explicit versus Implicit Spin Labels in the Context of Previous Approaches to Reproduce DEER Distance Distributions

Since the establishment of the four-pulsed EPR method to a more widespread application (Jeschke, 2002), it has been a major aim to describe and understand the flexibility of the MTS spin label in relation to the observed distance distributions to draw conclusions back to protein structure and dynamics. While there are only a limited number of experimentally determined spin label conformations, the conformational space accessible due to the five rotatable bonds is considerably large. Different attempts were made to predict the flexibility and orientation of the spin label. This includes a tether-in-a-cone model to produce distributions of interelectron distances in the context of CW-EPR

Table 2. Individual Fits of Each of the 16 Crystal Structure Conformers to the Apo- and ZnAMPCP-Bound States of 5NT

Crystal Structure	Conformation	Score	
		Apo	ZnAMPCP
1HP1_A	open	0.36	1.12
1USH_A	open	0.37	1.12
2USH_A	open	0.31	1.00
2USH_B	open	0.30	1.01
1OID_A	open	0.35	1.06
1OID_B	open	0.29	1.01
1OIE_A	open	0.38	1.11
1OI8_A	intermediate	1.25	0.51
1OI8_B	intermediate	1.26	0.52
4WWL_A	intermediate	1.29	0.52
1HPU_A	closed	1.97	0.90
1HPU_B	closed	1.93	0.86
1HPU_C	closed	2.02	0.96
1HPU_D	closed	1.97	0.91
1HO5_A	closed	2.03	0.97
1HO5_B	closed	1.98	0.92

spectra (Hustedt et al., 2006), Monte Carlo conformational searching of docked spin labels in combination with MD simulations (Sale et al., 2002, 2005), systematic studies on ensembles of rotamers (Guo et al., 2007, 2008), and usage of rotamer libraries as in MMM (Polyhach et al., 2011), the PRONOX algorithm (Hatmal et al., 2012), analysis of spin label rotamers by mtsslWizard (Hagelueken et al., 2012), the restrained ensemble MD simulation methodology (Islam et al., 2013; Roux and Islam, 2013), the knowledge-based potential of the cone model (which together with Rosetta was employed for de novo structure calculations) (Alexander et al., 2008; Hirst et al., 2011), or full-atom representations from RosettaEPR (Alexander et al., 2013, 2014). In a recent study, the latter two models were compared and distance distributions were more accurately described with full-atom spin labels (Alexander et al., 2013). In addition, ensemble fitting has also been used in previous studies to characterize flexible inter-domain orientations in solution via DEER. For the Gi protein, it was shown that the rigid-body movement of the helical domain relative to the rest of the protein increases significantly in the rhodopsin-bound state compared with the basal state (Alexander et al., 2014). Nine models were generated via rigid-body docking and ensemble fitting to describe the inter-domain mobility, which however features a less dramatic domain opening compared with the $\beta 2$ adrenergic receptor-Gs crystal structure (Rasmussen et al., 2011).

In the current work, the full-atom spin label representation is better able to reproduce the experimental distance distributions, as described by S , than the cone model. However, the improvement comes at the cost of overfitting the data. Possibly, the implicit ensemble of spin label conformations provided by the cone model prevents specific conformations of the spin label from creating well-matching distances from a structure that is unknowably a suboptimal selection overall, as could occur in the case of the explicit full-atom spin label fitting and would result in better S and worse S_{free} as observed.

Methodological Implications and Limitations

In general, the preciseness of fits to the experimental distance distributions is limited by the following factors. As described, the conformational flexibility of the spin label results in a broadening of the distance peaks. Even more problematic are effects of the local environment of the spin label that limit its flexibility. This could result in a systematically shorter or longer distance distribution compared with the cone model, which assumes a free flexibility. However, the data did not indicate such a scenario, and the use of explicit full-atom models of the spin label would result in better fitting results if the spin label motion was highly restricted.

In addition, analyzing the primary DEER data is associated with deviations in the height and positions of the peaks in the distance distribution. A further potential source of systematic errors is the influence of the spin labels on the conformational equilibrium itself. Although the specific activities of the labeled 5NT variants were comparable with the wild-type enzyme, it cannot be ruled out that the spin labels change the population of the different states compared with the wild-type enzyme. Still, the comparison of the calculated and observed distance distributions (Figure S4) indicates no large outliers among the six variants.

By the introduction of S_{free} , it was possible to estimate the degree of overfitting of the data. However, the significance of S_{free} is affected by the limited number of data points (distance distributions). Furthermore, the data points are not completely independent as each distance distribution shares one of the two label positions with another data point. If this label position influences the conformational equilibrium, the overfitting contribution of one variant with this label position will also lower S_{free} since the label position is present in a second distance distribution.

We could show that it is possible to characterize the equilibrium of the three basic states (open, intermediate, and closed) with six distance distributions and the influence of a substrate analog on this equilibrium. For the characterization of smaller conformational changes within the open or closed states or for a characterization of the structures without the restraints from the crystal structures (i.e., starting from the docked conformers), more distance distributions would be necessary. Model calculations are required to help to define the influence of the number of distance distributions, errors in the accuracy of the distributions and outliers (influence of the spin label on the equilibrium) on the behavior of the ensemble fits.

In summary, we presented a new approach to characterize a conformational equilibrium of a domain motion in solution by combination of EPR spectroscopy, X-ray crystal structures, and computational analysis in the form of the ensemble fitting. 5NT is an attractive model system to further establish and evaluate this methodology, which is particularly attractive for larger or complex systems to study structures and conformational switches of large molecular assemblies.

EXPERIMENTAL PROCEDURES

Choice of Spin Label Sites for EPR Distance Distribution Measurements

The double cysteine mutants for SDSL-EPR distance measurements were designed to probe structure and dynamics along maximally independent

Table 3. Comparison of Ensemble Fitting of 5NT Distance Distributions with Explicit Full-Atom versus Implicit (Cone Model) Spin Labels Attached to the Crystal Conformers

Score			No. of Conformers		Explicit SL		
Explicit SL	Implicit SL	Apo	Explicit SL	Implicit SL	Ratio of Open Conformations	Ratio of Intermediate Conformations	Ratio of Closed Conformations
$S = 0.1966 \pm 0.0023$	$S = 0.2911 \pm 0.0000$	six distance distributions	30.0 ± 4.2	1.0 ± 0.0	100%	0%	0%
$S_{\text{LOO}} = 0.0878 \pm 0.0044$	$S_{\text{LOO}} = 0.0338 \pm 0.0000$	LOO 124/398	32.5 ± 3.9	1.0 ± 0.0	100%	0%	0%
$S_{\text{LOO}} = 0.0510 \pm 0.0070$	$S_{\text{LOO}} = 0.1062 \pm 0.0000$	LOO 124/452	24.7 ± 4.9	1.0 ± 0.0	96%	4%	0%
$S_{\text{LOO}} = 0.0935 \pm 0.0101$	$S_{\text{LOO}} = 0.0315 \pm 0.0000$	LOO 124/532	30.1 ± 4.9	1.0 ± 0.0	100%	0%	0%
$S_{\text{LOO}} = 0.1030 \pm 0.0075$	$S_{\text{LOO}} = 0.0453 \pm 0.0000$	LOO 191/398	28.1 ± 3.0	1.0 ± 0.0	100%	0%	0%
$S_{\text{LOO}} = 0.0445 \pm 0.0090$	$S_{\text{LOO}} = 0.0265 \pm 0.0000$	LOO 191/452	25.5 ± 4.5	1.0 ± 0.0	95%	5%	0%
$S_{\text{LOO}} = 0.1591 \pm 0.0087$	$S_{\text{LOO}} = 0.0477 \pm 0.0000$	LOO 191/532	37.2 ± 5.8	1.0 ± 0.0	91%	9%	0%
$S_{\text{free}} = 0.5389 \pm 0.0467$	$S_{\text{free}} = 0.2910 \pm 0.0000$	average	29.7 ± 4.5	1.0 ± 0.0	$97\% \pm 4\%$	$3\% \pm 4\%$	0%
ZnAMPCP							
$S = 0.1898 \pm 0.0031$	$S = 0.3110 \pm 0.0000$	six distance distributions	46.5 ± 4.2	3.4 ± 1.0	48%	32%	20%
$S_{\text{LOO}} = 0.0950 \pm 0.0066$	$S_{\text{LOO}} = 0.0195 \pm 0.0000$	LOO 124/398	44.6 ± 3.9	2.0 ± 0.0	45%	34%	20%
$S_{\text{LOO}} = 0.0618 \pm 0.0039$	$S_{\text{LOO}} = 0.0772 \pm 0.0000$	LOO 124/452	46.6 ± 6.6	2.0 ± 0.0	53%	29%	18%
$S_{\text{LOO}} = 0.1356 \pm 0.0051$	$S_{\text{LOO}} = 0.0594 \pm 0.0000$	LOO 124/532	59.7 ± 3.6	3.2 ± 1.0	53%	29%	18%
$S_{\text{LOO}} = 0.0394 \pm 0.0032$	$S_{\text{LOO}} = 0.0192 \pm 0.0000$	LOO 191/398	44.4 ± 7.5	2.0 ± 0.0	44%	40%	17%
$S_{\text{LOO}} = 0.093 \pm 0.0092$	$S_{\text{LOO}} = 0.0476 \pm 0.0000$	LOO 191/452	44.2 ± 4.9	2.0 ± 0.0	44%	37%	19%
$S_{\text{LOO}} = 0.0459 \pm 0.0034$	$S_{\text{LOO}} = 0.0884 \pm 0.0006$	LOO 191/532	48.2 ± 7.4	2.4 ± 0.8	51%	31%	18%
$S_{\text{free}} = 0.4707 \pm 0.0314$	$S_{\text{free}} = 0.3110 \pm 0.0006$	average	47.7 ± 5.4	2.4 ± 0.8	$48\% \pm 4\%$	$33\% \pm 4\%$	$19\% \pm 1\%$

Results were obtained at $w_E = 0$ (explicit) and $w_E = 40$ (implicit). The average S and S_{LOO} are given as well as the average number of models of the best 10% of the fits with their SD. The last column shows the conformational composition of the ensemble after fitting with explicit full-atom spin labels for the best fit.

distance vectors within the known open and closed state structures in order to yield optimal information on the three-dimensional inter-domain orientations. For determination of appropriate positions, the structure of PDB: 1HP1 was chosen as the open conformer, and PDB: 1HO5 (chain A) as the closed state. The following criteria were applied to all pairs of labeling sites selected:

- (1) C_β distances in the open and closed state needed to be between 15 and 50 Å, which is the optimal range for DEER experiments thereby maximizing the accuracy of the experimental distance distributions;
- (2) the mutated residue must not be proline or cysteine (read below) to avoid disruption of the backbone conformation or an increase of flexibility of the protein;
- (3) the label must be located in an exposed position to avoid disruption of the backbone conformation of the protein;
- (4) the label should preferentially be located within a secondary structure element to minimize dynamics from conformational changes in loop regions, which was not a focus of the present study;
- (5) the distance change from the open to the closed conformation was maximized in order to increase the usefulness of the experiment to monitor the conformational change;
- (6) labeling sites were reused as much as possible to limit the number of mutants that had to be created and tested;
- (7) and at the same time, no two spin label pairs must connect the same two regions of the protein to avoid redundancy in the experimental setup.

Our protocol to achieve conditions 1–7 was as follows. First, all pairs of sites that fulfill criteria 1–4 were collected in a list. Next, the list was sorted by expected change in distance (criterion 5) and the top residue pair was chosen as the first double mutant. For the second distance, the list was pruned by removing pairs that did not contain one of the original labeling sites (criterion 6) and for pairs that link similar regions (criterion 7). Spin label pairs

were defined as linking similar regions if the respective pairs of C_β atoms were both closer than 15 Å. From the remaining pairs of residues, the one with the largest distance change was selected. This procedure was repeated until the list was empty.

An initial set of double mutants was selected and prepared. However, mutants with spin labels attached to L123C or A449C resulted in up to 80% reduced specific enzymatic activity and reduced flexibility of the spin label side chains as observed in CW-EPR experiments (data not shown). Therefore these spin label positions were excluded. The final set consisted of the six mutants T124C/G398C, T124C/Q452C, T124C/K532C, K191C/G398C, K191C/Q452C, and K191C/K532C. 5NT contains a natural disulfide C258/C275, which was also present in all EPR spin label mutants. A control experiment via labeling of the wild-type enzyme showed that the background labeling of the natural disulfide C258/C275 was less than 1% and thereby did not disturb the experiments.

Preparation of MTSSL-Labeled 5NT Mutants

The six 5NT variants each containing two additional cysteines were labeled with MTSSL. The experimental procedure is detailed in the [Supplemental Information](#). Briefly, after expression in *E. coli* and chromatographic purification (Schultz-Heinenbrok et al., 2004; Krug et al., 2013), a tenfold excess of MTSSL over protein was added in two steps with incubation at room temperature and 4°C. Unreacted spin label was removed by a desalting column.

Data Acquisition of EPR Distance Distributions

CW-EPR experiments were carried out on a Bruker EMX spectrometer using a 10-mW microwave power level and a modulation amplitude of 1.6 G. DEER spectroscopy was performed on a Bruker 580 pulsed EPR spectrometer operating at Q-band frequency (33.9 GHz) with a standard four-pulse protocol at 83 K (Jeschke, 2002). Data were processed in DeerAnalysis 2011 (Jeschke et al., 2006) with Tikhonov regularization and L-curve determination of the optimal

regularization parameter (Chiang et al., 2005). For 5NT sample details, see Supplemental Experimental Procedures.

Simulation of EPR Distance Distributions with a Rotamer Library

A rotamer library approach as implemented in the software MMM was used to predict the conformational space of the MTSSL (Polyhach et al., 2011). Based on these spin label rotamers, theoretical DEER distance distributions and expected mean distances between the MTSSL sites were predicted and compared with the experimentally obtained 5NT distance distributions.

Characterization of the Inter-domain Orientation

5NT conformations were characterized by a comparison with models generated along an ideal linear rotational path (i.e., rotation around a single axis) between the most open (1HP1_A, $\chi_1 = 97^\circ$) and the most closed conformer (1HPU_C, $\chi_1 = 0^\circ$). These artificial models were generated in steps of 1° rotation for a range of χ_1 from -50° to 200° . To characterize the conformational state of a given conformer relative to 1HPU_C, the conformer was superposed onto each conformer of the linear path by aligning first the N-terminal and then the C-terminal domains with the program LSQKAB (Kabsch, 1976). Thereby, a tilt angle χ_2 to each of the linear path models was calculated. Each conformer is thus finally characterized by the domain opening angle χ_1 of the closest reference state on the 1HPU_C-1HP1_A rotation and a tilt angle χ_2 , which describes the deviation from the reference state (as an inter-domain rotation angle). A χ_2 of 0° indicates a conformer on the 1HPU_C – 1HP1_A rotational path.

Conformers from the Crystal Structures

Eight crystal forms provided 16 independent 5NT conformers: PDB: 1USH, 2USH, 1HP1, 1O1D, 1O1E, 1O18, 1HO5, 1HPU, 4WWL (Knöfel and Sträter, 1999, 2001a, 2001b; Schultz-Heienbrok et al., 2004). They are indicated by their PDB ID and the respective protein chain (e.g., conformer 1HPU_C is chain C of 1HPU).

Conformers from a Targeted Molecular Dynamics Simulation

Three hundred conformers were taken from a targeted MD simulation between the open (1USH_A) and closed form of 5NT (1HPU_D) (U.K., N.S., unpublished data). The simulation results in a closure motion that runs via the crystallographically observed intermediate states.

Conformers from Domain Docking

Further models were created by docking of the domain structures, either from the most open (1HP1_A) or from the most closed crystallographic conformer (1HPU_C). Residues 26–353 and 363–550 were used for the N- and C-terminal domains, respectively. Docking was carried out with the Biochemical Library (BCL) using a protocol adapted from protein folding (Karakas et al., 2012) and allowed the domains to move as rigid bodies relative to one another. The linker helix of residues 354–362 was omitted, but a loop score (Woetzel et al., 2012) was employed in order to ensure the domains remained within biologically probable orientations of one another during docking.

Preparation of Full-Atom Spin Label Models

Fifty independent structure relaxation trajectories were conducted for each of the 16 crystal structures using the Rosetta relaxation protocol (Bradley et al., 2005). Next, a full-atom representation of MTSSL was attached to 5NT at residue sites 124, 191, 398, 452, and 532 of the 800 different relaxed conformers (Alexander et al., 2013). The Rosetta fixed backbone design protocol was used to perform the residue mutations and to optimize conformations of all side chains in the structure (Kuhlman et al., 2003).

Ensemble Fitting of Protein Models to EPR Distance Distributions

A Monte Carlo procedure was used to find the ensemble of protein models that best reproduces the experimentally measured EPR distance distributions. The models were selected from three different pools of structures: (1) the experimental crystal structures, (2) from a targeted MD simulation between the open and closed form, and (3) from domain docking. Several copies of these conformers served as the candidate pool with 1,500–3,000 protein models. The ensemble was selected from this pool. One protein model could be used several times in the final ensemble to represent an increased probability for that state.

The agreement of the ensemble with an individual EPR distance distribution is calculated based on the cumulative Euclidian distance (Kamarainen et al., 2003):

$$d = \sqrt{\frac{\sum_{b=0}^{B-1} \left(\sum_{j=0}^b \text{Ensemble}_j - \sum_{j=0}^b \text{EPR}_j \right)^2}{B}}$$

Here, B is the number of bins in the histograms describing the probability distributions for a given distance; Ensemble_j and EPR_j are the distance probabilities at bins j of the model ensemble and EPR distance distribution histograms, respectively. The cumulative Euclidian distance is normalized to the number of bins, and all distance distributions were scored across a range from 0 to 90 \AA .

For each EPR distance measured, a distance probability histogram for the ensemble of models is derived by implicitly representing the spin label in the protein models. For each model in the ensemble, the distance between the corresponding C_β atoms is converted into a probability distribution of likely spin label distances using the cone model and statistics previously described (Hirst et al., 2011). The ensemble distribution for a given distance is then the sum of the individual model probability distributions and corresponds to Ensemble from above. This procedure allows ensemble and EPR distances to be directly compared, since both will now correspond to spin label distances. When models with explicit spin labels are used, an ensemble's distribution for a given distance is directly calculated from the distances between spin labels within the structures of the ensemble. The score of the ensemble compared with all the EPR distances is the summation of d for each EPR measurement, $S = \sum_i d$.

An additional scoring term selects for small ensemble sizes. This ensures that only protein conformations critical to reproducing the experimental measurements are included in the ensemble. The ensemble size score is calculated as $E = N/P$, where N is the number of models in the ensemble and P is the constant total number of models in the candidate pool of models.

The total score of the ensemble $T = S + w_E E$ is calculated at each Monte Carlo step and determines whether an ensemble change will be accepted or rejected. The constant w_E is the weight of the size score. The smaller the total ensemble score T , the more accurately the ensemble reproduced all of the EPR measurements.

The ensemble was built up from an initial size of between 100 and 105 models using three possible changes to the ensemble: (1) adding a protein model from the pool to the current ensemble; (2) removing a protein model from the current ensemble; (3) swapping a protein model between the model pool and the current ensemble. At each Monte Carlo step, a change is applied and either accepted, if the move causes the ensemble to better reproduce the EPR distance distributions (reduced T), or rejected otherwise.

A relative improvement I was calculated after each move as $I = (T_{\text{old}} - T_{\text{new}})/T_{\text{new}}$. If a move is rejected, I is zero as T does not change. If the move is accepted, I gives the fraction of the improvement relative to the new score as a positive number as $T_{\text{old}} > T_{\text{new}}$. The Monte Carlo procedure terminated after T did not improve by 0.01 within 1,000 steps.

Leave-One-Out Validation Score

A leave-one-out score (S_{LOO}) was introduced to assess the degree of overfitting. For this, a leave-one-out-ensemble was determined by ensemble fitting against $(i - 1)$ distance distributions, i.e., against five of the six distance distributions. Then, S_{LOO} for the sixth (i.e., the left-out) distance distribution was determined by assessing the fit of the ensemble to the left-out distance distribution. This score describes the agreement with the distance distribution that was not used in fitting and is thus free from overfitting to this distance distribution. A free score value is calculated as $S_{\text{free}} = \sum_i S_{\text{LOO}}$ (Figure 5A).

SUPPLEMENTAL INFORMATION

Supplemental Information includes Supplemental Experimental Procedures, five figures, and three tables and can be found with this article online at <http://dx.doi.org/10.1016/j.str.2015.11.007>.

ACKNOWLEDGMENTS

S. Moschütz is acknowledged for support in purification of the first variants. This work was funded by the Deutsche Forschungsgemeinschaft. Work in the Meiler laboratory was supported through NIH (R01 GM080403, R01 MH090192, R01 GM099842) and NSF (Career 0742762). We thank the DAAD for funding a research exchange for U.K. and Vanderbilt University for N.S.

Received: July 24, 2015

Revised: October 20, 2015

Accepted: November 13, 2015

Published: December 24, 2015

REFERENCES

- Alexander, N., Bortolus, M., Al-Mestarihi, A., Mchaourab, H., and Meiler, J. (2008). De novo high-resolution protein structure determination from sparse spin-labeling EPR data. *Structure* 16, 181–195.
- Alexander, N.S., Stein, R.A., Koteiche, H.A., Kaufmann, K.W., Mchaourab, H.S., and Meiler, J. (2013). RosettaEPR: rotamer library for spin label structure and dynamics. *PLoS One* 8, e72851.
- Alexander, N.S., Preininger, A.M., Kaya, A.I., Stein, R.A., Hamm, H.E., and Meiler, J. (2014). Energetic analysis of the rhodopsin-G-protein complex links the α 5 helix to GDP release. *Nat. Struct. Mol. Biol.* 21, 56–63.
- Antonoli, L., Pacher, P., Vizi, E.S., and Hasko, G. (2013). CD39 and CD73 in immunity and inflammation. *Trends Mol. Med.* 19, 355–367.
- Bradley, P., Misura, K.M., and Baker, D. (2005). Toward high-resolution de novo structure prediction for small proteins. *Science* 309, 1868–1871.
- Chiang, Y.W., Borbat, P.P., and Freed, J.H. (2005). Maximum entropy: a complement to Tikhonov regularization for determination of pair distance distributions by pulsed ESR. *J. Magn. Reson.* 177, 184–196.
- Columbus, L., and Hubbell, W.L. (2002). A new spin on protein dynamics. *Trends Biochem. Sci.* 27, 288–295.
- Edwards, S.J., Moth, C.W., Kim, S., Brandon, S., Zhou, Z., Cobb, C.E., Hustedt, E.J., Beth, A.H., Smith, J.A., and Lybrand, T.P. (2014). Automated structure refinement for a protein heterodimer complex using limited EPR spectroscopic data and a rigid-body docking algorithm: a three-dimensional model for an ankyrin-CDB3 complex. *J. Phys. Chem. B* 118, 4717–4726.
- Fan, J., Zhang, Y., Chuang-Smith, O.N., Frank, K.L., Guenther, B.D., Kern, M., Schlievert, P.M., and Herzberg, M.C. (2012). Ecto-5'-nucleotidase: a candidate virulence factor in *Streptococcus sanguinis* experimental endocarditis. *PLoS One* 7, e38059.
- Fanucci, G.E., and Cafiso, D.S. (2006). Recent advances and applications of site-directed spin labeling. *Curr. Opin. Struct. Biol.* 16, 644–653.
- Firon, A., Dinis, M., Raynal, B., Poyart, C., Trieu-Cuot, P., and Kaminski, P.A. (2014). Extracellular nucleotide catabolism by the Group B *Streptococcus* ectonucleotidase NudP increases bacterial survival in blood. *J. Biol. Chem.* 289, 5479–5489.
- Glaser, L., Melo, A., and Paul, R. (1967). Uridine diphosphate sugar hydrolase. Purification of enzyme and protein inhibitor. *J. Biol. Chem.* 242, 1944–1954.
- Guo, Z., Cascio, D., Hideg, K., Kálái, T., and Hubbell, W.L. (2007). Structural determinants of nitroxide motion in spin-labeled proteins: tertiary contact and solvent-inaccessible sites in helix G of T4 lysozyme. *Protein Sci.* 16, 1069–1086.
- Guo, Z., Cascio, D., Hideg, K., and Hubbell, W.L. (2008). Structural determinants of nitroxide motion in spin-labeled proteins: solvent-exposed sites in helix B of T4 lysozyme. *Protein Sci.* 17, 228–239.
- Hagelueken, G., Ward, R., Naismith, J.H., and Schiemann, O. (2012). MtsslWizard: in silico spin-labeling and generation of distance distributions in PyMOL. *Appl. Magn. Reson.* 42, 377–391.
- Hatmal, M.M., Li, Y., Hegde, B.G., Hegde, P.B., Jao, C.C., Langen, R., and Haworth, I.S. (2012). Computer modeling of nitroxide spin labels on proteins. *Biopolymers* 97, 35–44.
- Heuts, D.P., Weissenborn, M.J., Olkhov, R.V., Shaw, A.M., Gummadova, J., Levy, C., and Scrutton, N.S. (2012). Crystal structure of a soluble form of human CD73 with ecto-5'-nucleotidase activity. *Chembiochem* 13, 2384–2391.
- Hirst, S.J., Alexander, N., Mchaourab, H.S., and Meiler, J. (2011). RosettaEPR: an integrated tool for protein structure determination from sparse EPR data. *J. Struct. Biol.* 173, 506–514.
- Hubbell, W.L., Cafiso, D.S., and Altenbach, C. (2000). Identifying conformational changes with site-directed spin labeling. *Nat. Struct. Biol.* 7, 735–739.
- Hustedt, E.J., Stein, R.A., Sethaphong, L., Brandon, S., Zhou, Z., and Desensi, S.C. (2006). Dipolar coupling between nitroxide spin labels: the development and application of a tether-in-a-cone model. *Biophys. J.* 90, 340–356.
- Islam, S.M., Stein, R.A., Mchaourab, H.S., and Roux, B. (2013). Structural refinement from restrained-ensemble simulations based on EPR/DEER data: application to T4 lysozyme. *J. Phys. Chem. B* 117, 4740–4754.
- Jeschke, G. (2002). Distance measurements in the nanometer range by pulse EPR. *Chemphyschem* 3, 927–932.
- Jeschke, G. (2012). DEER distance measurements on proteins. *Annu. Rev. Phys. Chem.* 63, 419–446.
- Jeschke, G., Chechik, V., Ionita, P., Godt, A., Zimmermann, H., Banham, J., Timmel, C.R., Hilger, D., and Jung, H. (2006). DeerAnalysis2006 - a comprehensive software package for analyzing pulsed ELDOR data. *Appl. Magn. Reson.* 30, 473–498.
- Kabsch, W. (1976). A solution for the best rotation to relate two sets of vectors. *Acta Crystallogr. A* 32, 922–923.
- Kamarainen, J.K., Kyrki, V., Ilonen, J., and Kälviäinen, H. (2003). Improving similarity measures of histograms using smoothing projections. *Pattern Recognit. Lett.* 24, 2009–2019.
- Karakas, M., Woetzel, N., Staritzbichler, R., Alexander, N., Weiner, B.E., and Meiler, J. (2012). BCL: fold-de novo prediction of complex and large protein topologies by assembly of secondary structure elements. *PLoS One* 7, e49240.
- Knapp, K., Zebisch, M., Pippel, J., El-Tayeb, A., Müller, C.E., and Sträter, N. (2012a). Crystal structure of the human ecto-5'-nucleotidase (CD73): insights into the regulation of purinergic signaling. *Structure* 20, 2161–2173.
- Knapp, K.M., Zebisch, M., and Sträter, N. (2012b). Crystallization and preliminary X-ray analysis of the open form of human ecto-5'-nucleotidase (CD73). *Acta Crystallogr. Sect. F Struct. Biol. Cryst. Commun.* 68, 1545–1549.
- Knöfel, T., and Sträter, N. (1999). X-Ray structure of the *Escherichia coli* periplasmic 5'-nucleotidase containing a dimetal catalytic site. *Nat. Struct. Biol.* 6, 448–453.
- Knöfel, T., and Sträter, N. (2001a). *E. coli* 5'-nucleotidase undergoes a hinge-bending domain rotation resembling a ball-and-socket motion. *J. Mol. Biol.* 309, 255–266.
- Knöfel, T., and Sträter, N. (2001b). Mechanism of hydrolysis of phosphate esters by the dimetal center of 5'-nucleotidase based on crystal structures. *J. Mol. Biol.* 309, 239–254.
- Krug, U., Patzschke, R., Zebisch, M., Balbach, J., and Sträter, N. (2013). Contribution of the two domains of *E. coli* 5'-nucleotidase to substrate specificity and catalysis. *FEBS Lett.* 587, 460–466.
- Kuhlman, B., Dantas, G., Ireton, G.C., Varani, G., Stoddard, B.L., and Baker, D. (2003). Design of a novel globular protein fold with atomic-level accuracy. *Science* 302, 1364–1368.
- Liu, P., Pian, Y., Li, X., Liu, R., Xie, W., Zhang, C., Zheng, Y., Jiang, Y., and Yuan, Y. (2014). *Streptococcus suis* adenosine synthase functions as an effector in evasion of PMN-mediated innate immunity. *J. Infect. Dis.* 210, 35–45.
- Mchaourab, H., Steed, P.R., and Kazmier, K. (2011). Toward the fourth dimension of membrane protein structure: insight into dynamics from spin-labeling EPR spectroscopy. *Structure* 19, 1549–1561.
- Neu, H.C. (1967). The 5'-nucleotidase of *Escherichia coli*. I. Purification and properties. *J. Biol. Chem.* 242, 3896–3904.
- Polyhach, Y., Bordignon, E., and Jeschke, G. (2011). Rotamer libraries of spin labelled cysteines for protein studies. *Phys. Chem. Chem. Phys.* 13, 2356–2366.

- Rasmussen, S.G.F., DeVree, B.T., Zou, Y., Kruse, A.C., Chung, K.Y., Kobilka, T.S., Thian, F.S., Chae, P.S., Pardon, E., Calinski, D., et al. (2011). Crystal structure of the β_2 adrenergic receptor-Gs protein complex. *Nature* *477*, 549–555.
- Roux, B., and Islam, S.M. (2013). Restrained-ensemble molecular dynamics simulations based on distance histograms from double electron-electron resonance spectroscopy. *J. Phys. Chem. B* *117*, 4733–4739.
- Ruiz, A., Hurtado, C., Meireles, R.J., Sillero, A., and Gunther Sillero, M.A. (1989). Hydrolysis of bis(5'-nucleosidyl) polyphosphates by *Escherichia coli* 5'-nucleotidase. *J. Bacteriol.* *171*, 6703–6709.
- Sale, K., Sár, C., Sharp, K.A., Hideg, K., and Fajer, P.G. (2002). Structural determination of spin label immobilization and orientation: a Monte Carlo minimization approach. *J. Magn. Reson.* *156*, 104–112.
- Sale, K., Song, L., Liu, Y.-S., Perozo, E., and Fajer, P. (2005). Explicit treatment of spin labels in modeling of distance constraints from dipolar EPR and DEER. *J. Am. Chem. Soc.* *127*, 9334–9335.
- Schultz-Heienbrok, R., Maier, T., and Sträter, N. (2004). Trapping a 96 degrees domain rotation in two distinct conformations by engineered disulfide bridges. *Protein Sci.* *13*, 1811–1822.
- Schultz-Heienbrok, R., Maier, T., and Sträter, N. (2005). A large hinge bending domain rotation is necessary for the catalytic function of *Escherichia coli* 5'-nucleotidase. *Biochemistry* *44*, 2244–2252.
- Thammavongsa, V., Kern, J.W., Missiakas, D.M., and Schneewind, O. (2009). *Staphylococcus aureus* synthesizes adenosine to escape host immune responses. *J. Exp. Med.* *206*, 2417–2427.
- Ward, R., Zoltner, M., Beer, L., El Mkami, H., Henderson, I.R., Palmer, T., and Norman, D.G. (2009). The orientation of a tandem POTRA domain pair, of the beta-barrel assembly protein BamA, determined by PELDOR spectroscopy. *Structure* *17*, 1187–1194.
- Woetzel, N., Karakas, M., Staritzbichler, R., Muller, R., Weiner, B.E., and Meiler, J. (2012). BCL: score-knowledge based energy potentials for ranking protein models represented by idealized secondary structure elements. *PLoS One* *7*, e49242.
- Zimmermann, H. (1992). 5'-Nucleotidase: molecular structure and functional aspects. *Biochem. J.* *285*, 345–365.
- Zimmermann, H., Zebisch, M., and Sträter, N. (2012). Cellular function and molecular structure of ecto-nucleotidases. *Purinergic Signal.* *8*, 437–502.

Structure, Volume 24

Supplemental Information

**Characterization of the Domain Orientations
of *E. coli* 5'-Nucleotidase by Fitting an Ensemble
of Conformers to DEER Distance Distributions**

Ulrike Krug, Nathan S. Alexander, Richard A. Stein, Antje Keim, Hassane S. Mchaourab, Norbert Sträter, and Jens Meiler

Supplemental Data

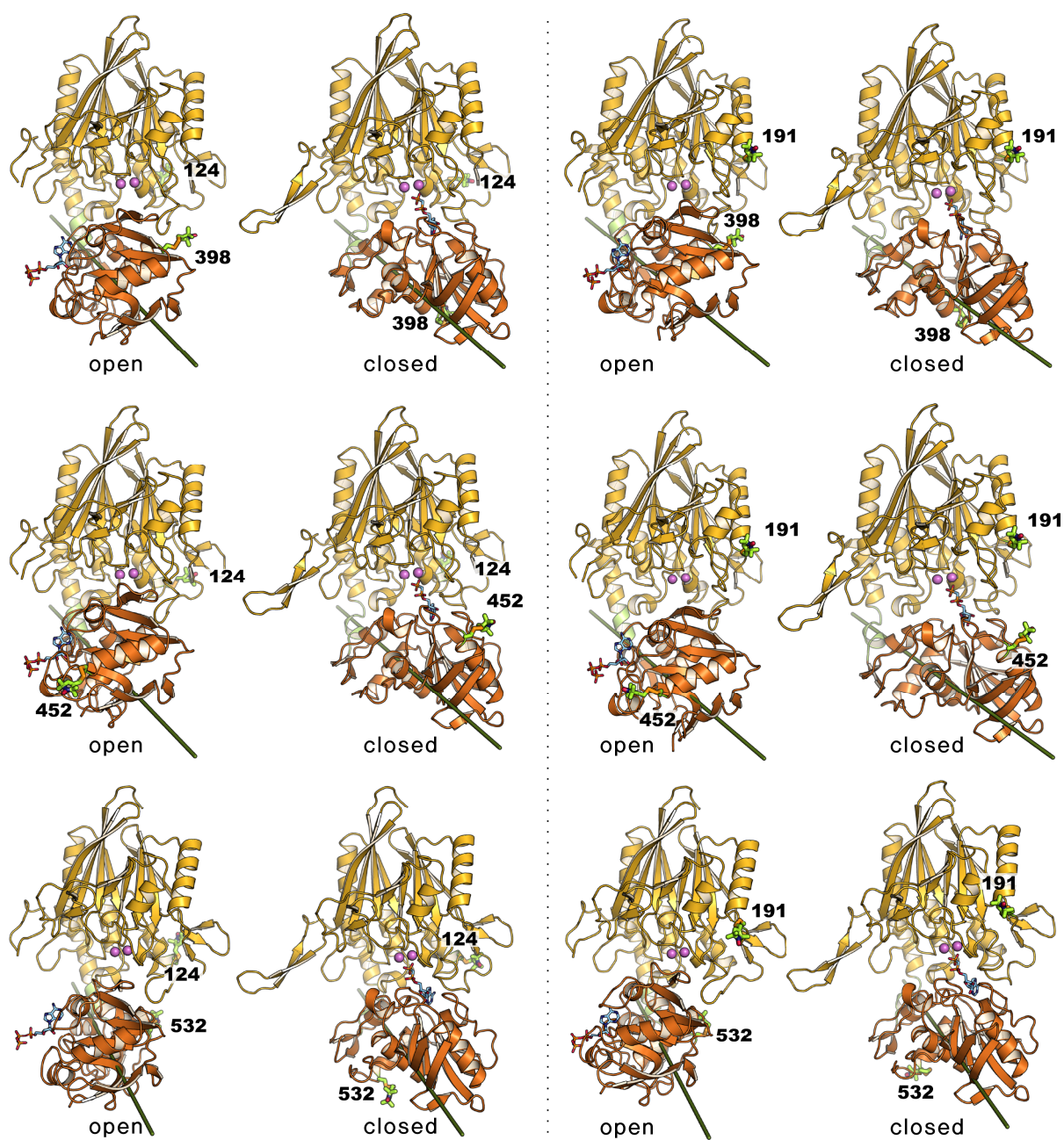


Figure S1 (related to Figure 1): 5NT variants in the open and closed conformations labeled with MTSSL. Six double cysteine mutants were prepared: T124C/G398C, T124C/Q452C, T124C/K532C, K191C/G398C, K191C/Q452C and K191C/K532C. The line through the center of the C-terminal domain marks the rotation axis between the two states.

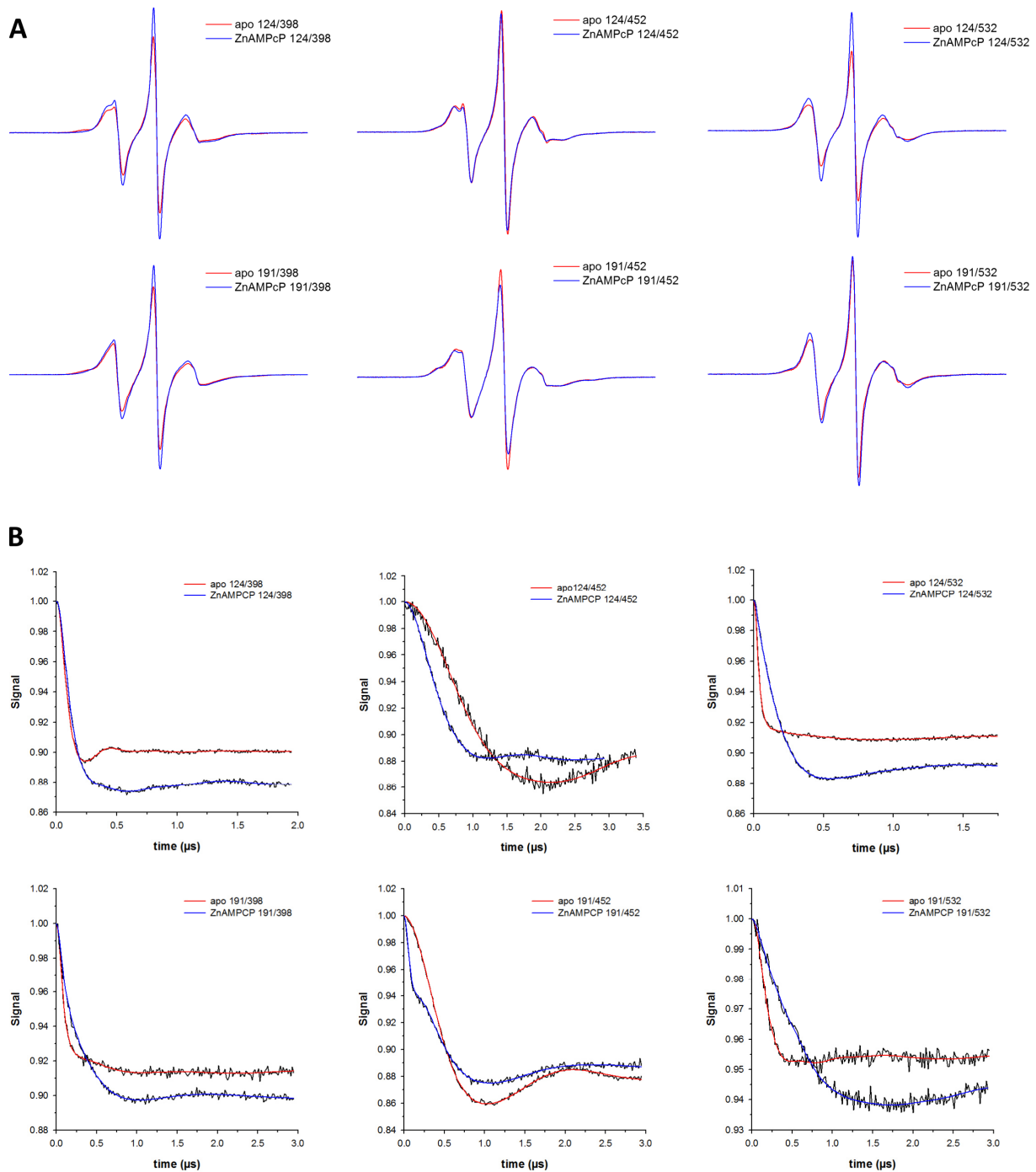
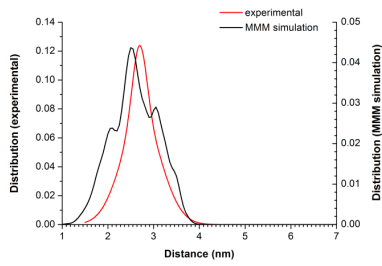
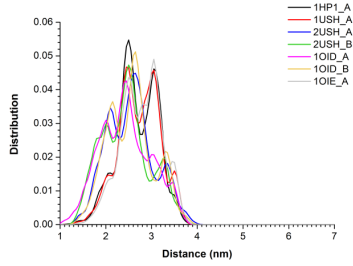
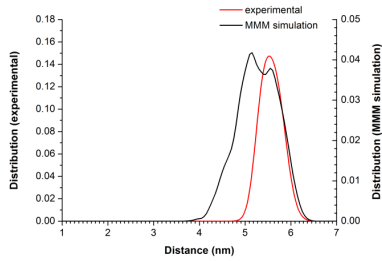
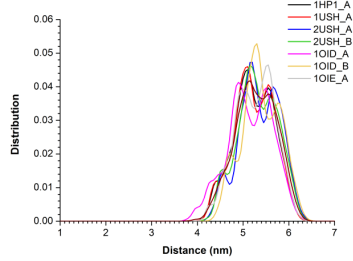


Figure S2 (related to Figure 2): CW-EPR spectra and DEER traces of MTSSL labeled 5NT variants in the apo (red) and ZnAMPCP-bound state (blue). A) CW-Spectra were collected on a Bruker EMX spectrometer using 10 mW microwave power level and a modulation amplitude of 1.6 G. B) DEER spectroscopy was performed on a Bruker 580 pulsed EPR spectrometer operating at Q-band frequency (33.9 GHz) with a standard four-pulse protocol at 83 K. Numbers indicate spin-labeled 5NT mutants T124C/G398C, T124C/Q452C, T124C/K532C, K191C/G398C, K191C/Q452C and K191C/K532C.

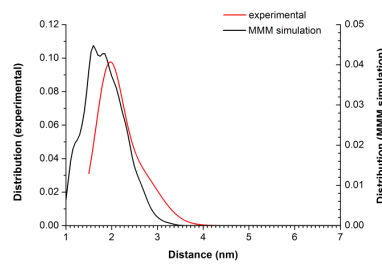
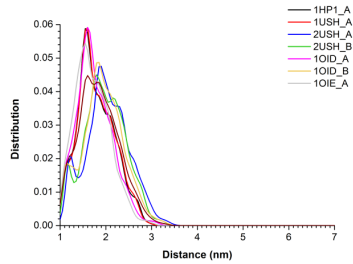
MTSSL labeling at residues 124/398



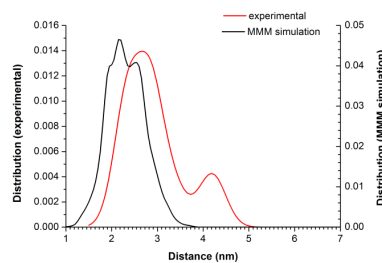
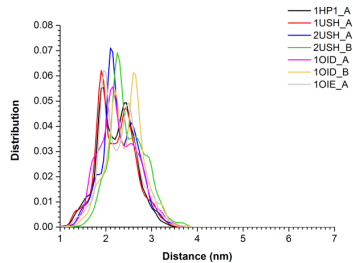
MTSSL labeling at residues 124/452



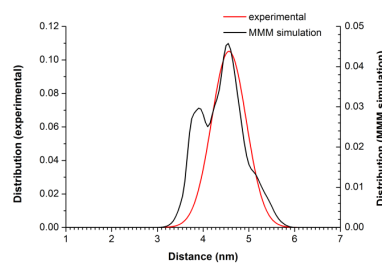
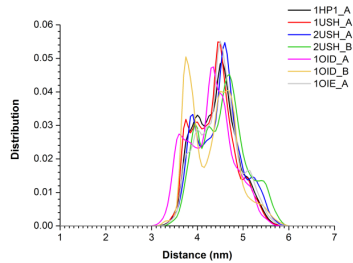
MTSSL labeling at residues 124/532



MTSSL labeling at residues 191/398



MTSSL labeling at residues 191/452



MTSSL labeling at residues 191/532

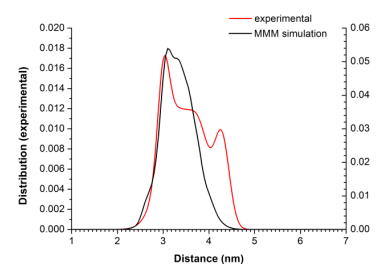
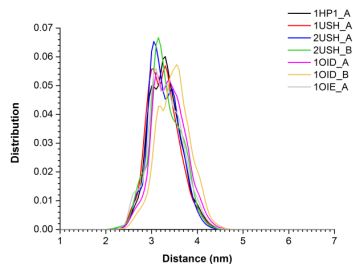
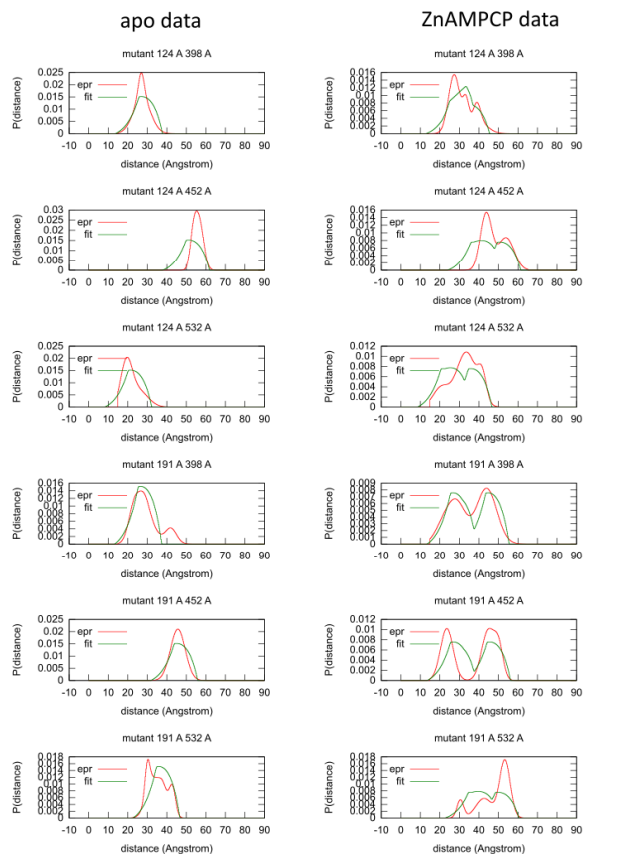


Figure S3 (related to Figure 2): Simulation of DEER distance distributions for 5NT variants with rotamer library from MMM. The program MMM was used to simulate the distance distributions of the six 5NT double mutants for seven open conformations (left). The “average” distance distribution of the seven open conformations is compared to the experimentally obtained DEER data (right).

Ensemble fit with crystal structures

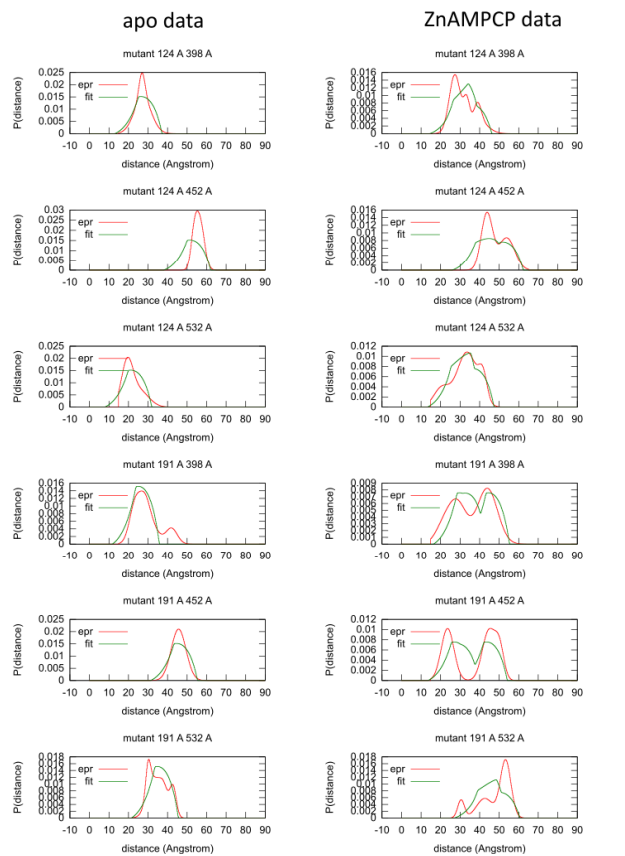


bcl::storage:Table<double>	weight	value	weighted_val	bcl::storage:Table<double>	weight	value	weighted_val
mutant_124_A_398_A	1.0000	0.0338	0.0338	mutant_124_A_398_A	1.0000	0.0195	0.0195
mutant_124_A_452_A	1.0000	0.1062	0.1062	mutant_124_A_452_A	1.0000	0.0772	0.0772
mutant_124_A_532_A	1.0000	0.0315	0.0315	mutant_124_A_532_A	1.0000	0.0594	0.0594
mutant_191_A_398_A	1.0000	0.0453	0.0453	mutant_191_A_398_A	1.0000	0.0192	0.0192
mutant_191_A_452_A	1.0000	0.0265	0.0265	mutant_191_A_452_A	1.0000	0.0476	0.0476
mutant_191_A_532_A	1.0000	0.0477	0.0477	mutant_191_A_532_A	1.0000	0.0881	0.0881
ensemble_size	40.0000	0.0006	0.0250	ensemble_size	40.0000	0.0013	0.0013
sum	46.0000	0.2916	0.3160	sum	46.0000	0.3122	0.3610

ensemble:
1× 1OID_open_B

ensemble:
1× 2USH_open_B
1× 1HPU_closed_A

Ensemble fit with MD models

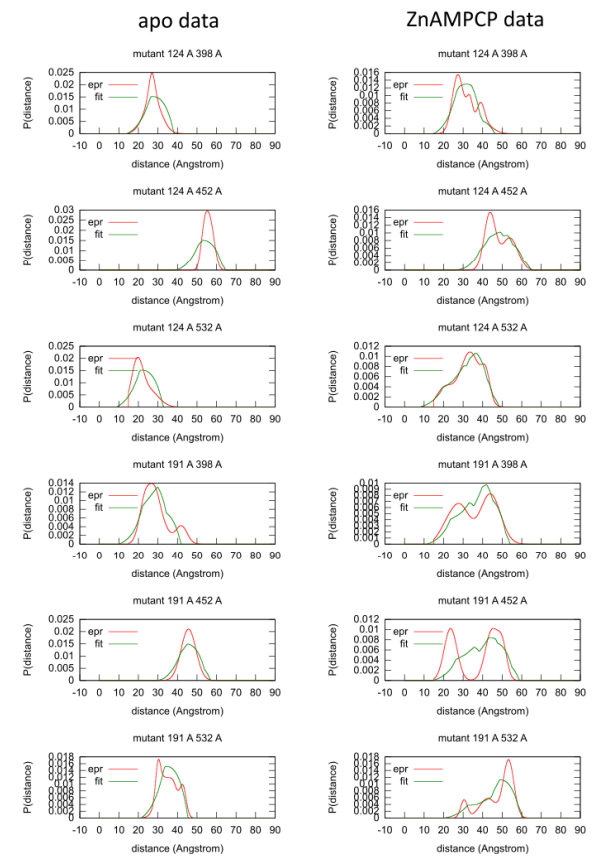


bcl::storage:Table<double>	weight	value	weighted_val	bcl::storage:Table<double>	weight	value	weighted_val
mutant_124_A_398_A	1.0000	0.0250	0.0250	mutant_124_A_398_A	1.0000	0.0342	0.0342
mutant_124_A_452_A	1.0000	0.1014	0.1014	mutant_124_A_452_A	1.0000	0.0485	0.0485
mutant_124_A_532_A	1.0000	0.0268	0.0268	mutant_124_A_532_A	1.0000	0.0145	0.0145
mutant_191_A_398_A	1.0000	0.0678	0.0678	mutant_191_A_398_A	1.0000	0.0423	0.0423
mutant_191_A_452_A	1.0000	0.0229	0.0229	mutant_191_A_452_A	1.0000	0.0627	0.0627
mutant_191_A_532_A	1.0000	0.0250	0.0250	mutant_191_A_532_A	1.0000	0.0637	0.0637
ensemble_size	40.0000	0.0007	0.0267	ensemble_size	40.0000	0.0013	0.0533
sum	46.0000	0.2696	0.2956	sum	46.0000	0.2672	0.3192

ensemble: X1 (X2)
1×MD-27 93° (3.1°)

ensemble: X1 (X2)
1× MD-54 78° (4.1°)
1× MD-280 7° (2.6°)

Ensemble fit with docked models



bcl::storage:Table<double>	weight	value	weighted_val	bcl::storage:Table<double>	weight	value	weighted_val
mutant_124_A_398_A	1.0000	0.0429	0.0429	mutant_124_A_398_A	1.0000	0.0220	0.0220
mutant_124_A_452_A	1.0000	0.0679	0.0679	mutant_124_A_452_A	1.0000	0.0249	0.0249
mutant_124_A_532_A	1.0000	0.0402	0.0402	mutant_124_A_532_A	1.0000	0.0090	0.0090
mutant_191_A_398_A	1.0000	0.0302	0.0302	mutant_191_A_398_A	1.0000	0.0320	0.0320
mutant_191_A_452_A	1.0000	0.0268	0.0268	mutant_191_A_452_A	1.0000	0.0830	0.0830
mutant_191_A_532_A	1.0000	0.0228	0.0228	mutant_191_A_532_A	1.0000	0.0369	0.0369
ensemble_size	40.0000	0.0007	0.0267	ensemble_size	40.0000	0.0013	0.0533
sum	46.0000	0.2315	0.2575	sum	46.0000	0.2093	0.2613

ensemble: X1 (X2)
1× c19 60° (28.9°)
1× o437 110° (21.2°)

ensemble: X1 (X2)
1× c170 14° (8.0°)
1× o375 38° (16.5°)
1× o331 67° (6.4°)
1× o84 122° (21.6°)

Figure S4 (related to Figure 3): Ensemble fit of 5NT EPR distance distributions with crystal structures, MD and docked models. The experimental data (red) and the fit with the given ensemble (green) are plotted for the apo and the ZnAMPCP data. Histograms are shown for ensemble fitting with a weight for the ensemble size (w_E) of 40. Statistics reflect the contribution of each mutant to the total score T (“sum”) in ensemble fitting. The composition of each ensemble is given.

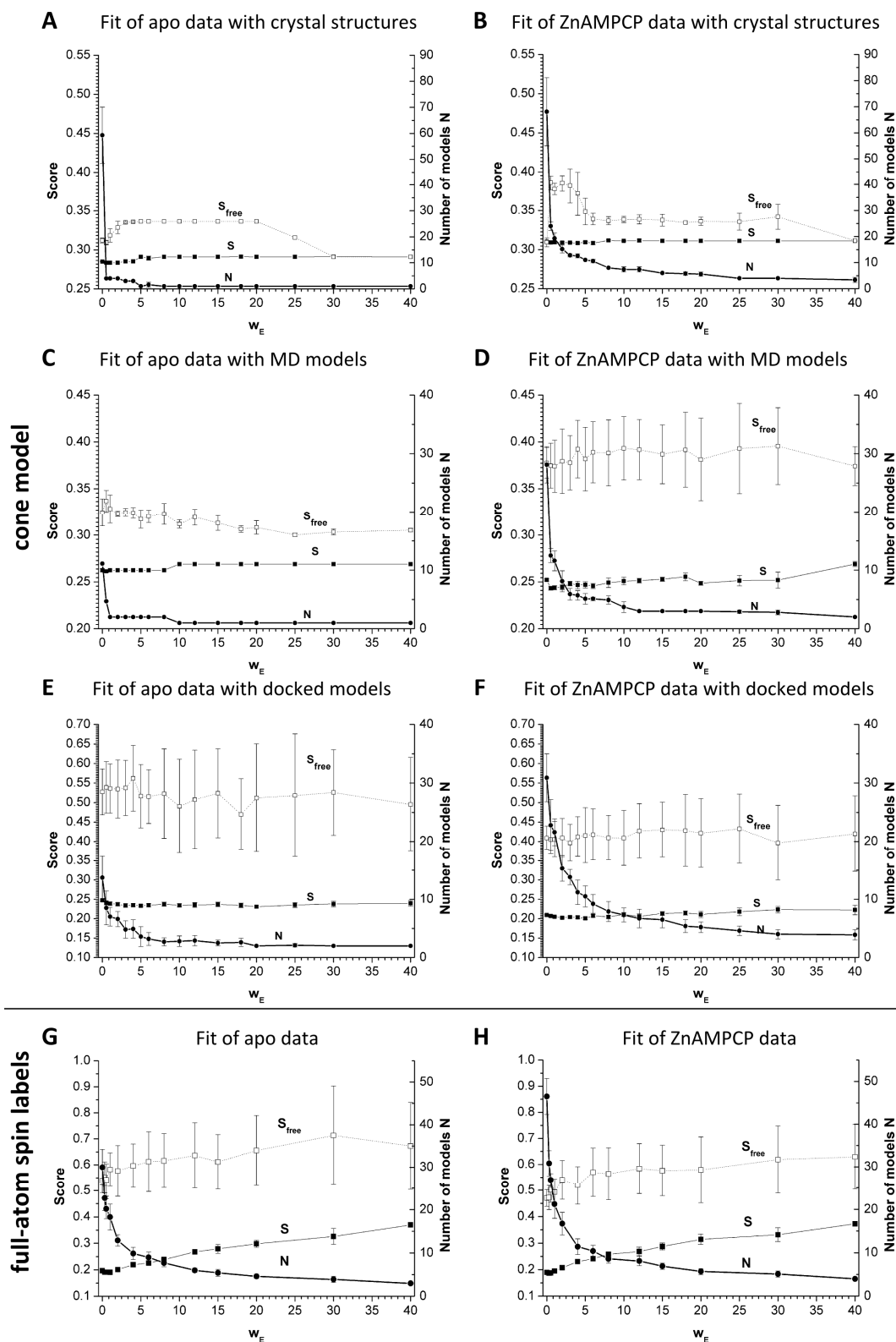


Figure S5 (related to Figure 5): Ensemble fitting based on the knowledge-based potential of the cone model (A-F) or with full-atom models of MTSSL attached to 5NT crystal structures (G-H). Given is the dependency of the Score (S), the free Score (S_{free}) and the number of models in the ensemble (N) on the weighting term for the ensemble size score (w_E). Distance distributions of 5NT in the apo and in the inhibitor-bound ZnAMPCP state were ensemble fitted with crystal structures, MD models or docked models for different w_E . Indicated values are the average of the best 10% of the fits with their standard deviations. For each weighting term the resulting S (-■-), S_{free} (··□··) and N (-●-) is given.

Table S1 (Related to Figure 4): Classification of 300 models derived from targeted MD simulation of the 5NT domain motion. The classification is based on the χ_1 angle as defined by the linear path analysis of the closed-to-open-rotation of structures 1HPU_C to 1HP1_A.

Classification of MD-models	Range of MD-models	Rotational range χ_1
open	MD-1 to MD-45, MD-47	$105.5 \leq \chi_1 \leq 80.0^\circ$
int. 1	MD46, MD-48 to MD-66	$80.0^\circ < \chi_1 \leq 65.0^\circ$
int. 2	MD-67 to MD-90	$65.0^\circ < \chi_1 \leq 50.0^\circ$
int. 3	MD-91 to MD-141	$50.0^\circ < \chi_1 \leq 35.0^\circ$
int. 4	MD-142 to MD-167, MD-169, MD-172, MD-174, MD-175	$35.0^\circ < \chi_1 \leq 20.0^\circ$
closed	MD-168, MD-170, MD-171, MD-173, MD-176 to MD-300	$20.0^\circ < \chi_1 \leq 0.0^\circ$

Table S2: Classification of 1000 models derived from docking of the N- and C-terminal domains of 5NT (Related to Figure 4). The classification is based on the χ_1 angle as defined by the linear path analysis of the closed-to-open-rotation of structures 1HPU_C to 1HP1_A.

	Classification of docked models	Rotational range χ_1
1	more-open	$105^\circ < \chi_1$
2	Open	$105^\circ \leq \chi_1 \leq 80^\circ$
3	int. 1	$80^\circ < \chi_1 \leq 65^\circ$
4	int. 2	$65^\circ < \chi_1 \leq 50^\circ$
5	int. 3	$50^\circ < \chi_1 \leq 35^\circ$
6	int. 4	$35^\circ < \chi_1 \leq 20^\circ$
7	Closed	$20^\circ < \chi_1 \leq -5^\circ$
8	more-closed	$-5^\circ > \chi_1$

Table S3 (Related to Table 1): Detailed summary of the results of the best LOO-fit for crystal structures, MD models and models from docking of the domains at a weighting term $w_E = 40$.

crystal struct.	apo				ZnAMPCP			
	ensemble	Score			ensemble	Score		
all	1OID_B	0.291			1HPU_A 2USH_B	0.311		
124/398	1OID_B	0.0338			1HPU_A 2USH_B	0.0195		
124/452	1OID_B	0.1062			1HPU_A 2USH_B	0.0772		
124/532	1OID_B	0.0315			1HPU_A 2USH_B	0.0594		
191/398	1OID_B	0.0453			1HPU_A 2USH_B	0.0192		
191/452	1OID_B	0.0265			1HPU_A 2USH_B	0.0476		
191/532	1OID_B	0.0477			1HPU_A 2USH_B	0.0881		
MD models	apo				ZnAMPCP			
	ensemble	χ_1	χ_2	Score	ensemble	χ_1	χ_2	Score
all	MD-27	93°	3.1°	0.2689	MD-280 MD-54	7° 78°	2.6° 4.1°	0.2759
124/398	MD-27	93°	3.1°	0.0250	MD-180 MD-54	15° 78°	6.5° 4.1°	0.0435
124/452	MD-28	92°	4.0°	0.1076	MD-277 MD-54	7° 78°	2.2° 4.1°	0.0591
124/532	MD-27	93°	3.1°	0.0268	MD-280 MD-35	7° 90°	2.6° 4.3°	0.0570
191/398	MD-27	93°	3.1°	0.0678	MD-280 MD-54	7° 78°	2.6° 4.1°	0.0423
191/452	MD-27	93°	3.1°	0.0229	MD-173 MD-54	18° 78°	9.0° 4.1°	0.0873
191/532	MD-37	89°	4.1°	0.0557	MD-295 MD-35	7° 90°	5.0° 4.3°	0.0890
docking models	apo				ZnAMPCP			
	ensemble	χ_1	χ_2	Score	ensemble	χ_1	χ_2	Score
all	o437 c19	110° 60°	21.2° 28.9°	0.2308	o84 o331 o375 c170	122° 67° 38° 14°	21.6° 6.4° 16.5° 8.0°	0.208
124/398	o437 c19	110° 60°	21.2° 28.9°	0.0429	o437 o331 c242 c65	110° 67° 20° 19°	21.2° 6.4° 13.4° 11.1°	0.0232
124/452	o429 c19	147° 60°	39.1° 28.9°	0.1657	o473 o465 c340 c45	144° 85° 20° 11°	34.5° 7.6° 10.7° 17.3°	0.1110
124/532	o437 c19	110° 60°	21.2° 28.9°	0.0402	o104 o465 c242 c65	126° 85° 20° 19°	42.6° 7.6° 13.4° 11.1°	0.0131
191/398	o437	110°	21.2°	0.0995	c82 o216 c355 c182	76° 54° 46° -3°	16.2° 33.3° 23.4° 8.7°	0.0803
191/452	o264 c19	122° 60°	23.8° 28.9°	0.0478	o84 o331 c435 o161	122° 67° 46° 27°	21.6° 6.4° 4.2° 14.4°	0.1365
191/532	o437 c19	110° 60°	21.2° 28.9°	0.0228	o342 c341 c92	97° 40° -7°	12.1° 14.8° 6.2°	0.1005

Supplemental Experimental Procedures

Preparation of 5NT mutants used for EPR spin labeling

To prepare the six 5NT double cysteine mutants T124C/G398C, T124C/Q452C, T124C/K532C, K191C/G398C, K191C/Q452C and K191C/K532C the gene coding for 5NT cloned in the pET28a(+) vector (Krug et al., 2013) was modified by site-directed mutagenesis via the QuikChange Mutagenesis protocol (Stratagene). The following sense mutagenesis primers were used: 5'-GAT AAT CCG CTC TGC GTA TTA CGC CAG CAG G-3' for T124C, 5'-GAT ATC GAA TTT CGT TGC CCC GCC GAT GAA GCG AAG C-3' for K191C, 5'-C CAA ATG GAT CGC ACT TGC GCC GAC TTT GCG GTG-3' for G398C, 5'-CTG ACC GCC GTC GCG TGC ATG AAG CCA GAT TCA GG-3' for Q452C and 5'-G CTG AAA GCG TAT ATC CAG TGC AGC TCG CCG CTG GAT GTG-3' for K532C (point mutations are underlined). The modified 5NT genes containing the natural disulfide C258/C275 plus two additional cysteines were expressed in *E. coli* BL21(DE3) or Rosetta pLysS cells. The 25 amino acid long signal sequence was cleaved off after secretion into the periplasm resulting in a protein of amino acids Y26 to Q550, with the introduced mutations and followed by the artificial C-terminal LEHHHHHH-sequence. Purification was carried out as described before by affinity, ion exchange and size exclusion chromatography (Schultz-Heienbrok et al., 2004; Krug et al., 2013). 1 mM DTT was added to all buffers during purification of the protein to prevent formation of disulfides by the artificial cysteines.

The specific enzymatic activity (U/mg) was determined by the release of phosphate after enzymatic turnover of AMP using a modified malachite green assay as detailed before (Krug et al., 2013).

Coupling of MTSSL to free cysteine residues

1-oxyl-2,2,5,5-tetramethylpyrroline-3-methyl methanethiosulfonate (MTSSL, purchased from Toronto Research Canada via LGC Standards GmbH, Wesel/Germany) was dissolved in anhydrous DMF and stored as 100 mM stock solution at -80°C. For labeling the protein buffer was changed to 9 mM Tris, 6 mM MES, 50 mM NaCl, 0.1 mM EDTA and 3 mM NaN₃ (pH 7.2) on a 5 mL HiTrap Desalting column (GE Healthcare) to remove DTT. Then a tenfold excess of MTSSL over protein was added, followed by two hours of incubation at room temperature and another addition of MTSSL

(again a tenfold excess). The mixture was incubated at 4°C over night. Finally, unreacted spin label was removed by a 53 mL HiTrap Desalting column (GE Healthcare) with 20 mM Tris, 50 mM KCl and 0.5 mM EDTA (pH 8.5).

Data acquisition of EPR distance distributions

After labeling protein samples were frozen in liquid nitrogen and transferred to Nashville on dry ice within 3 days. Glycerol (30% w/w) was added as cryoprotectant. To provide samples in the inhibitor-bound state 5 mM AMPCP (Sigma Aldrich/Germany) and 0.5 mM ZnCl₂ were added before freezing. Due to a K_i of 0.25 μM the concentration of AMPCP corresponds to a saturating amount of inhibitor. For CW-EPR, spin-labeled 5NT samples were loaded in capillaries and spectra were collected on a Bruker EMX spectrometer using a 10 mW microwave power level and a modulation amplitude of 1.6 G. DEER spectroscopy was performed on a Bruker 580 pulsed EPR spectrometer operating at Q-band frequency (33.9 GHz) with a standard four-pulse protocol at 83 K (Jeschke, 2002). Analysis of the DEER data to determine the distance distributions, P(r), was carried out in DeerAnalysis 2011 (Jeschke et al., 2006). The data were fitted with Tikhonov regularization and L-curve determination of the optimal regularization parameter (Chiang et al., 2005).

Supplemental References

Chiang, Y.W., Borbat, P.P., and Freed, J.H. (2005). Maximum entropy: a complement to Tikhonov regularization for determination of pair distance distributions by pulsed ESR. *J.Magn Reson.* *177*, 184-196.

Jeschke, G. (2002). Distance measurements in the nanometer range by pulse EPR. *Chemphyschem.* *3*, 927-932.

Jeschke, G., Chechik, V., Ionita, P., Godt, A., Zimmermann, H., Banham, J., Timmel, C.R., Hilger, D., and Jung, H. (2006). DeerAnalysis2006- a comprehensive software package for analyzing pulsed ELDOR data. *Applied Magnetic Resonance* *30*, 473-498.

Krug, U., Patzschke, R., Zebisch, M., Balbach, J., and Sträter, N. (2013). Contribution of the two domains of *E. coli* 5'-nucleotidase to substrate specificity and catalysis. *FEBS Lett.* *587*, 460-466.

Schultz-Heienbrok, R., Maier, T., and Sträter, N. (2004). Trapping a 96 degrees domain rotation in two distinct conformations by engineered disulfide bridges. *Protein Sci.* *13*, 1811-1822.